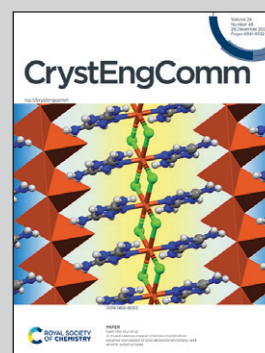**Showcasing research from Dr Joanna Bojarska's laboratory, Chemistry Department, Institute of Ecological and Inorganic Chemistry, Technical University of Lodz, 116 Zeromskiego St., 90-924 Lodz, Poland.**

Supramolecular synthon hierarchy in cyclopropyl-containing peptide-derived compounds

A combined experimental-computational study of five novel cyclopropyl-containing peptide-derived compounds is focussed on the synthons preferences in (bio)supramolecular architecture. The potential of π-based cyclopropyl synthon is discussed too. As a bonus, promising activity of new molecules against prostate cancer is revealed.

As featured in:

See Joanna Bojarska *et al.*, *CrystEngComm*, 2022, **24**, 8372.

ROYAL SOCIETY OF **CHEMISTRY**

rsc.li/crystengcomm

Check for updates

Supramolecular synthon hierarchy in cyclopropyl-containing peptide-derived compounds†

Joanna Bojarska, [iD] *[a] Martin Breza, [iD] [b] Milan Remko,[c] Paweł Borowiecki, [iD] [d] Andrzej Fruziński,[a] Izabela D. Madura, [iD] [e] Krzysztof Kaczmarek,[f] Zbigniew Leśnikowski,[gh] Agata Kraj,[h] Piotr Zielenkiewicz[ij] and Wojciech M. Wolf[a]

Considering the increasing importance of cyclopropyl-containing peptide-derived compounds in the pharmaceutical industry, herein, we report the crystal engineering of a series of novel derivatives, *i.e.*, diethyl 2-acetamido-2-(cyclopropylmethyl)malonate (1), 2-(cyclopropylmethyl)-2-acetamidopropanedioic acid (2) [Ac-*b*-cyclopropyl-(*R,S*)-Ala-OH], 2-(cyclopropylmethyl)-2-acetamidopropanedioic acid hydrate (3), 2-acetamido-3-cyclopropylpropanoic acid (4), and (2*S*)-2-[cyclopropyl(9*H*-fluoren-9-ylmethoxycarbonyl)amino]propanoic acid (5) [Fmoc-*b*-cyclopropyl-(*S*)-Ala-OH]. Although several cyclopropyl-based peptide-derived structures have been reported in the literature, to the best of our knowledge, studies on the synthon hierarchy in this class of structures are limited. Thus, to address this gap, herein, we report a multidisciplinary study to shed light on the role of cyclopropyl synthons in (bio)supramolecular assemblies, opening a new vista for the further applications of this unique scaffold. The synthesis was achieved *via* a multi-step protocol in good yield and the structures were determined by single-crystal X-ray diffraction. The diverse supramolecular synthons responsible for the arrangement of molecules in the crystal lattice of either new compounds or all cyclopropyl-containing peptide-derived solids deposited in the CSD thus far were specified and summarized, building a library. The self-assembly is directed by the cooperative interplay of H-bonds and π-stacking interactions. Quantum-chemical computational studies revealed that the cyclopropyl ring is capable of $\pi_{(C=O)}\cdots\sigma^*_{(cyclopropyl)}$, $\pi_{(arom)}\cdots\sigma^*_{(cyclopropyl)}$, $\pi^*_{(arom)}\cdots\sigma^*_{(cyclopropyl)}$ and $\pi^*_{(arom)}\cdots\sigma_{(cyclopropyl)}$ interactions. The molecular docking study delineated the C–H$\cdots$C$_{(cyclopropyl)}$ and C–H$_{(cyclopropyl)}\cdots\pi$ interactions of the cyclopropyl moiety with the essential amino acid residues inside the active pocket of the human androgen receptor, highlighting the vital role of cyclopropyl in the supramolecular landscape of the bio-complex. Indeed, 2 shows a significant docking score with effective binding affinity, and thus is a promising candidate for prostate cancer prevention or management.

[a] *Chemistry Department, Institute of Ecological and Inorganic Chemistry, Technical University of Lodz, 116 Zeromskiego St., 90-924 Lodz, Poland. E-mail: joanna.bojarska@p.lodz.pl*

[b] *Department of Physical Chemistry, Slovak Technical University, Radlinskeho 9, SK-81237 Bratislava, Slovakia*

[c] *Remedika, Luzna 9, SK-85104, Bratislava, Slovakia*

[d] *Laboratory of Biocatalysis and Biotransformation, Department of Drugs Technology and Biotechnology, Faculty of Chemistry, Warsaw University of Technology, 75 Koszykowa St., 00-662 Warsaw, Poland*

[e] *Faculty of Chemistry, Warsaw University of Technology, 3 Noakowskiego St., 00-664 Warsaw, Poland*

[f] *Institute of Organic Chemistry, Faculty of Chemistry, Lodz University of Technology, 116 Zeromskiego St., 90-924 Lodz, Poland*

[g] *Institute of Medical Biology, Polish Academy of Sciences, Laboratory of Medicinal Chemistry, 106 Lodowa St., 92-232 Lodz, Poland*

[h] *Institute of Medical Biology, Polish Academy of Sciences, National Library of Chemical Compounds POL-OPENSCREEN, 106 Lodowa St., 92-232 Lodz, Poland*

[i] *Institute of Biochemistry and Biophysics, Polish Academy of Sciences, Pawinskiego 5a, 02-106 Warsaw, Poland*

[j] *Department of Systems Biology, Institute of Experimental Plant Biology and Biotechnology, University of Warsaw, Miecznikowa 1, 02-096 Warsaw, Poland*

† Electronic supplementary information (ESI) available. CCDC 2203890–2203894. For ESI and crystallographic data in CIF or other electronic format see DOI: https://doi.org/10.1039/d2ce01231f

1. Introduction

Cyclopropyl is a unique motif attracting wide interests in synthetic, supramolecular, and medicinal chemistry, chemical biology, and molecular recognition processes due to its wide bio-applications and specific chemical nature, *i.e.*, coplanarity of carbon atoms, short C–H and C–C bonds, and enhanced π-character.[1–8] Interestingly, an extensive list of cyclopropyl-based drugs contains more than a hundred therapeutic agents related to cancers, infectious diseases (viral, bacterial, and fungal), cardiovascular, metabolic, neurological, skin, dental, and eye disorders, depression, and many other conditions.[9–27] Remarkably, about 20 peptide-derived compounds with the cyclopropyl moiety have been approved by the Food and Drug Administration (FDA) in the last decade[28] (Table S1†). Thus, cyclopropyl exists in ~10% of all new therapeutics, which together with fluorinated methyl (CF$_3$), is one of the most popular pharmaceutical scaffolds.[29,30] However, it should be highlighted that

fluorinated drugs are controversial due to the possible tissue-specific fluorination of proteins.[31] Alternatively, the small cyclopropyl system possesses appealing features such as increased potency, metabolic stability, brain permeability, reduced off-target effects, and plasma clearance[32] as well as enhanced cytotoxicity toward tumor cells.[33] Cyclopropyl may contribute to entropically more favorable binding to biological targets due to its conformational rigidity.[32] It is worth mentioning that cyclopropyl forms hydrophobic interactions with the protein target,[34] which can be amplified by π-based inter-contacts. Also, π-sigma interaction can help intercalate the ligand (drug) in the binding site and enhance the affinity between the ligand and receptor.[35] This can be one of the key issues in the explaining the differences in activity related to dynamic behavior.[36] Currently, peptide-derived compounds have gained increasing attention as safe and effective next-generation therapeutic agents due to their high affinity and excellent specificity towards protein receptors with recent progress in biotechnology overcoming their shortcomings.[37–39]

An understanding of the molecular topology and modification of the supramolecular framework is essential to design new drugs with the desired bio-pharmacokinetic properties due to their close relationship.[40] The behavior of drug molecules in bio-systems depends on the combination of H-bond acceptors and donors (and their molecular shape). Hirshfeld surface (HS) studies provide a valuable source of information on the supramolecular properties of potential bioactive substances. Interestingly, the HS concept is also being used to profile the shape of the protein pocket and generate the HS around the ligand molecule. Consequently, the design of effective ligand molecules inside the protein pocket by using proper H-bonding synthons[41] from the model library of interactions may be possible in the future.[42] A crystal is a supermolecule,[43] and a bio-complex can also be considered a supermolecule. In this context, the cyclopropyl-based synthon data are clearly needed, but to the best of our knowledge cyclopropyl-based supramolecular synthons have received much less attention to date.

The aim of this work was to hierarchize the supramolecular synthons responsible for the molecular arrangement in cyclopropyl-containing peptide-derived crystals. Specifically, a series of novel cyclopropyl-based modified amino acids and closely related compounds, i.e., diethyl 2-acetamido-2-(cyclopropylmethyl)malonate (**1**), 2-(cyclopropylmethyl)-2-acetamidopropanedioic acid (**2**) [Ac-b-cyclopropyl-(R,S)-Ala-OH], 2-(cyclopropylmethyl)-2-acetamidopropanedioic acid hydrate (**3**), 2-acetamido-3-cyclopropylpropanoic acid (**4**), and (2S)-2-[cyclopropyl(9H-fluoren-9-ylmethoxycarbonyl)amino]propanoic acid (**5**) [Fmoc-b-cyclopropyl-(S)-Ala-OH], were successfully synthesized, thoroughly investigated by solid-state structural analysis and theoretical calculations, and compared with structures deposited in the CSD, providing a library of H-bonding supramolecular motifs. Notably, we revealed the potential of

the cyclopropyl ring to create π-based supramolecular synthons. In addition, we evaluated the bio-pharmaceutical profiles of the new molecules using computational methods, and their binding modes in the active site of human androgen receptor (hAR) were rationalized via molecular docking analysis.

These studies fit into the mainstream of our ongoing project that concentrates on supramolecular exploration and bioactivity of peptide-based molecules.[37,38,44–82]

2. Experimental

2.1. Synthesis and single-crystal X-ray diffraction (SCXRD)

The synthesis of the novel compounds **1–5** was based on the literature[83] and our experience, which is discussed in the ESI† in detail.

X-ray diffraction data for compounds **1–5** were collected at 100 K on an XtaLAB Synergy Dualflex Pilatus 300 K diffractometer (Rigaku Corporation, Tokyo, Japan) and processed using the Olex2 software.[84] The structures were solved with SHELXT,[85] using CrysAlis PRO for data reduction,[86] and refined with SHELXL[87] using least-squares minimization. All non-hydrogen atoms were refined anisotropically and hydrogen atoms were positioned geometrically and refined with isotropic thermal displacement parameters $[U_{iso}(H) = 1.2U_{eq}(CH, CH_2)$ and $U_{iso}(H) = 1.5U_{eq}(CH_3)]$. The details of the X-ray measurements and crystal data for all the compounds studied are presented in Table 1. The CCDC No. of the title compounds **1–5** are as follows: CCDC 2203890 (**1**), 2203891 (**2**), 2203892 (**3**), 2203893 (**4**) and 2203894 (**5**).

Geometrical calculations were performed using the PLATON program,[88] while the crystal structure diagrams and analysis of H-bond graph-sets performed using Mercury 4.0.[89–91]

2.2. Computational details

2.2.1. Quantum-chemical calculations. The geometry of the neutral molecules C_3H_6, **1**, **2**, **4**, and **5** in the singlet ground state was completely optimized in the gas phase using the Gaussian09 software.[92] Density functional theory[93–95] was used with the M06 functional[96] and the 6-311++G(d,p) basis set for all atoms.[97] The stability of the optimized structures was verified by vibrational analysis (no imaginary vibrations). Natural bond orbital (NBO) analysis was performed using the NBO 3.1 program[98] in terms of natural charges for atoms and Wiberg indices for bonds. For the relevant C–C and C–H bonds, the contributions of the p electrons in the carbon sp^n hybrid orbitals was evaluated.[5] The banana bond[4] deviations α_i and α_j from the line connecting the C_i and C_j atoms, respectively, were used to evaluate the bent bond angle β_k as follows:

$$\beta_k = \gamma_k + \sum \alpha_k \qquad (1)$$

Table 1 Crystal structure data and structure refinement for compounds **1**–**5**

Compound	1	2	3	4	5
Empirical formula	$C_{13}H_{21}NO_5$	$C_9H_{13}NO_5$	$C_9H_{13}NO_5$, H_2O	$C_8H_{13}NO_3$	$C_{21}H_{21}NO_4$
Formula weight	271.31	215.20	233.22	171.19	351.39
Crystal system	Orthorhombic	Triclinic	Orthorhombic	Monoclinic	Monoclinic
Space group	$Pna2_1$	$P\bar{1}$	$Pbca$	P_12_1/c_1	I_12_1
a (Å)	9.589(2)	7.49868(19)	13.72920(10)	14.66220(10)	24.5330(2)
b (Å)	12.661(3)	8.0934(2)	10.90840(10)	11.42930(10)	5.04577(4)
c (Å)	11.779(3)	9.4854(2)	14.82920(10)	21.61680(10)	30.1674(3)
α (°)	90	83.844(2)	90	90	90
β (°)	90	73.807(2)	90	90.6010(10)	109.5159(10)
γ (°)	90	69.194(3)	90	90	90
Volume (Å^3)	1430.0(6)	516.76(3)	2220.87(3)	3622.32(4)	3519.81(6)
Z	4	2	8	16	8
d_{calc} (mg m^{-3})	1.260	1.383	1.395	1.256	1.326
Wavelength	0.71073	0.71073	0.71073	0.71073	0.71073
T (K)	100(2)	100(2)	100(2)	100(2)	100(2)
No. of unique reflections	13 453	2043	2229	7387	6882
Absorption correction	None	Multi-scan	None	Gaussian	Gaussian
No. of refined parameters	257	140	152	442	518
No. of restraints	1	0	0	0	1
GOF on F^2	1.01317	1.05569	1.05542	1.04768	1.03688
R_1	0.0533	0.0282	0.0294	0.0353	0.0254
wR_2	0.1381	0.0719	0.0789	0.0930	0.0655
Min/max residual density	0.410/−0.442	0.360/−0.185	0.381/−0.247	0.362/−0.294	0.243/−0.151

where γ_k is the C_j–C_k–C_i angle in the cyclopropyl ring and α_k is two deviations of the banana bond at the same C_k atom. Stabilizing interactions[99,100] were evaluated for each donor i-th and acceptor j-th orbital associated with the $i \rightarrow j$ delocalization as follows:

$$E_{ij}^{(2)} = n_i \frac{F_{ij}^2}{\varepsilon_i - \varepsilon_j} \qquad (2)$$

where F_{ij} is the off-diagonal Fock matrix element between the i-th and j-th natural orbitals, ε_i and ε_j are their energies, and n_i is the donor orbital population.

Using the AIM2000 software[101] Quantum Theory of Atoms-in-Molecules (QTAIM),[102] atomic volumes and charges were calculated by integration over their atomic basins up to the 0.001 a.u. level. The QTAIM bond characteristics in terms of electron density, ρ, and its Laplacian, $\nabla^2\rho$, given by eqn (3)

$$\nabla^2\rho = \lambda_1 + \lambda_2 + \lambda_3 \qquad (3)$$

and bond ellipticity, ε, given by eqn (4):

$$\varepsilon = \lambda_1/\lambda_2 - 1 \qquad (4)$$

were calculated at the bond critical points (BCP), which are defined using zero gradients and the eigenvalues, λ_I, of the Hessian of the BCP electron density followed the order of $\lambda_1 < \lambda_2 < 0 < \lambda_3$. The $_{BCP}$ value is proportional to the bond strength; the covalent and dative bonding correspond to negative and positive $\nabla^2\rho_{BCP}$ values, respectively, and ε_{BCP}, describes its deviation from cylindrical symmetry due to its double-bond character, mechanical strain, and other perturbations.

2.2.2. Docking protocol. Molecular docking calculations were performed with AutoDock Vina vs. 1.1.2. program (https://autodock.scripps.edu/) using the standard docking protocol described in our recent study (for more details, see ESI†).[52] All ligands were prepared with ChemAxon MarvinSketch vs. 14.9.1.0 (https://www.chemaxon.com/marvin/), optimized in terms of geometry in Avogadro vs. 1.2.0. (https://avogadro.cc/), and saved as .mol2 files. The macromolecule target structure, hAR (PDB code: 1E3G, 2.40 Å resolution crystal structure of human androgen receptor), was taken from the RCSB Protein Data Bank (https://www.rcsb.org/). All non-protein molecules (i.e., ligand R1881 and crystal waters) were removed, polar hydrogens were added, and Gasteiger charges were calculated using AutoDock tools vs. 1.5.6. (https://mgltools.scripps.edu/) to obtain the appropriate file in .pdbqt format. Next, AutoGrid was used to find an appropriate grid box size. The grid box center was set at 0.802, 29.745, 3.780 (x, y, z coordinates respectively) with the following final size space dimension $x = 60$ Å, $y = 60$ Å, and $z = 60$ Å. The dockings were performed with an exhaustiveness level of 48. The receptor–ligand interactions were visualized using PyMOL Molecular Graphics System software vs. 1.3, Schrödinger, LLC (https://www.pymol.org/). The validation of the docking protocol was achieved by ensuring that the database ligand [metribolone (R1881)] could be re-docked to hAR under the established parameters, resulting in the same accommodation as in the co-crystallized hAR-1881 complex (PDB code: 1E3G).

2.2.3. Hirshfeld surface analysis. 3D electron density maps, known as Hirshfeld surfaces (HS),[42] 2D fingerprint plot (FP),[103] molecular electrostatic potential surface (EP),[104] and energy framework (EF)[105,106] calculations were performed using the CrystalExplorer21, v. 21.5.[107] The calculations were

based on the B3LYP/6-31G(d,p) model wavefunctions by employing the Tonto program[108] embedded in CrystalExplorer. The X-ray crystallographic information files (cif) for compounds **1–5** were used as input files, with the X–H bond lengths normalized to standard neutron diffraction values.

2.2.4. ADMET and beyond. The ADMET profiles for the studied compounds were calculated using SwissADME, a web-based interface, provided by the Molecular Modelling Group of the Swiss Institute of Bioinformatics[109,110] and the pkCSM web platform.[111] The bioactivity scores of the analyzed compounds were calculated using the online computer Molinspiration Cheminformatics software (https://www.molinspiration.com). Cardiovascular toxicity was predicted using the pred-hERG 4.2 web tool, which is freely available.[112] The tumor and non-tumor cell line cytotoxicity were investigated using the CLC-pred tool, which is based on structure-cell line cytotoxicity relationships by the PASS procedure (activity spectra for substances).[113] All *in silico* simulations were carried out in June 2022. The structures of the peptides were converted into canonical simplified molecular input line entry specifications (SMILES).

The pK_a and $\log P_{oct/w}$ measurements[114–117] for **5** are described in the ESI.†

2.3. CSD/PDB survey

A search of the CSD (ver. 5.43 updates March 2022)[118] was carried out using a cyclopropyl scaffold related to modified amino acids and peptide-related compounds. 225 crystal structures containing cyclopropyl were found, which confirmed the novelty of the synthesized compounds **1–5**. Next, we restricted the search in terms of the following filters: 3D coordinates determined, R factor ≤ 0.05, only non-disordered, no errors, not polymeric, only single crystal structures, only organics, and no repeated entries. Consequently, 33 crystal structures consisting of cyclopropyl were extracted. The CSD refcodes of these entries are as follows: ADELOM, ADELUS, ADEMAZ, ADEMED,[119] APOFOD,[120] BUTCIE,[121] CARYAY,[122] CATWEA,[123] CEGVUH,[124] CERQUM,[125] EDIWIZ,[126] FIJDIO,[127] GENYUU,[128] HILXIM,[129] HORZEU,[130] IHUFEY,[131] JAWLAU,[132] KEZNEJ,[133] KUDZIS,[134] LIKFIX,[135] MENHIW,[136] MOYSEB,[137] PEDWOM,[138] ROPQUL,[139] VEHDIY,[140] VETKEL,[141] WICMIH,[142] WOVXAG,[143] XICRAC,[144] ZAMJEF, ZAMJOP,[145] ZEGGEZ,[146] and ZUQBIY.[147] The molecular views and basic crystallographic data for the literature 'hits' are summarized in Tables S2 and S3,† respectively. It is noteworthily that no structure is a close relative of the new compounds **1–5**. Therefore, a detailed discussion of these structures, besides those of cyclopropyl-based synthons, is beyond the scope of this article.

Furthermore, in the Brookhaven RCSB Protein Data Bank (PDB database, https://www.rcsb.org/pdb/), 814 structures with cyclopropyl scaffolds have been deposited so far. Interestingly, 59 entries (Table S2†) of them were deposited this year.

3. Results and discussion

3.1. Structural description and supramolecular analysis

The perspective views of the molecular structures of **1–5** with the thermal ellipsoidal plots and the non-hydrogen atom labelling schemes are presented in Fig. S1,† while Scheme S1† shows the superposition of all the structures, revealing the similarities of **1–3**, and differences between **4** and **5**. The molecule of **4** has R and S chiral centres at C3, C3A, C3B, and C3C, while in **5** has S at C3 and C3A. In **5**, the fluorenyl methoxycarbonyl (Fmoc) group and the carbamate linkages [N–C9(O3)–O4–C10/NA–C9A(O3A)–O4A–C10A] are planar. In all the compounds, the amide bonds are in a *trans* conformation. The structures are stabilized by diverse intra-N–H⋯O, C–H⋯O and intermolecular O–H⋯O, N–H⋯O, C–H⋯O and H–bonding interactions, in the range of 2.5342(1) Å in **3** to 3.5379(1) Å in **4** due to the presence of rich H-bonding donors and acceptors, mainly in terms of amine, carbonyl, and carboxylic groups. H-bonds with a distance of D–A ≤2.55 Å for O–H⋯O (observed in **2–4**) and ≤2.65 Å for N–H⋯O (in **1–3**) are called short strong H-bonds. Interestingly, all the h-atoms of the NH and OH groups and O atoms of the C=O groups in all the reported compounds are involved in the H-bonding as donors and acceptors, respectively (only in **2** a weak NH⋯C bond is observed). The geometric parameters of the H-bonding interactions are collected in Table 2, while the π-stacking interactions in **5** are shown in Table S4† (π⋯π) and Table S5† (C–H⋯π). Notably, the H⋯Cg distances are in the range of 2.53–2.83 Å, and according to Malone,[148] the C–H⋯π hydrogen bonds are classified as type I.

To gain deeper insight into the supramolecular preferences of the novel structures in the context of all the cyclopropyl-containing peptide-derived compounds known thus far, 33 entries from the CSD, described in the Experimental section and included in Tables S2 and S3,† were re-analyzed and considered. Consequently, with these additional crystal data, we identified the main basic synthons, highlighting the new H-bonding motifs realized for the first time in novel compounds **1–5**. However, obtaining appropriate information was a challenge because of the complexity of the CSD structures with diverse functional groups with multiple H-bond donors and acceptors. All the identified types of both non-cyclopropyl- and cyclopropyl-based supramolecular interactions (synthons) are presented in Fig. 1 and S2,† respectively. Interestingly, the molecules show a greater preference for hetero- than homo-synthons. The cyclic motifs are built by $_{carboxyl}$O–H⋯O$_{carbonyl/carboxyl}$, N–H⋯O$_{carbonyl}$ and $_{aryl}$C–H⋯O$_{carbonyl/carboxyl}$ interactions. Linear H-bonding patterns are created by $_{hydroxyl/carboxyl}$O–H⋯O$_{carbonyl}$, N–H⋯O$_{carbonyl}$, $_{aryl}$C–H⋯O$_{carbonyl/carboxyl}$, $_{aryl}$C–H⋯O$_{hydroxyl}$, S–H⋯S–H, and $_{aryl}$C–H⋯S–H. The H-bonding synthon motifs called B3 and B5 are formed by N–H⋯O$_{carbonyl}$ and $_{aryl}$C–H⋯O$_{carbonyl}$, respectively, as well as the bifurcated synthon C1 resulting from the most popular in this class of compounds. At this point, more attention can be

Table 2 Hydrogen bond parameters in **1–5** (bonding and non-bonding distances bond lengths are in Å and D–H⋯A angles in degrees)

D–H⋯A	d(D–H)	d(H⋯A)	d(D⋯A)	(DHA)
1				
N–H⋯O4[a]	0.86	2.29	2.6579(7)	106
N–H⋯O1[i]	0.86	2.12	2.9565(8)	162
C2–H2A⋯O1[i]	0.96	2.39	3.2680(8)	152
C2–H2B⋯O4[ii]	1.00	2.43	3.3481(9)	151
C4–H4B⋯O5[a]	0.99	2.57	2.9123(7)	100
C10–H10C⋯O4[iii]	0.96	2.54	3.1685(8)	123

(i) −1/2 + x, ½ − y, z; (ii) 1 − x, −y, −1/2 + z; (iii) ½ + x, ½ − y, z.

D–H⋯A	d(D–H)	d(H⋯A)	d(D⋯A)	(DHA)
2				
N–H⋯O2[a]	0.86	2.23	2.6273(1)	108
N–H⋯O2[i]	0.86	2.41	3.0318(1)	130
O3–H3⋯O1[ii]	0.82	1.78	2.5893(1)	170
O5–H5⋯O4[iii]	0.82	1.84	2.6590(1)	177
C2–H2A⋯O2[iv]	0.96	2.37	3.2729(1)	156
C5–H5A⋯O2[i]	0.98	2.57	3.4524(1)	150

(i) 1 + x, y, z (ii) −1 + x, y, z; (iii) −x, 1 − y, 2 − z; (iv) 1 − x, −y, 1 − z

D–H⋯A	d(D–H)	d(H⋯A)	d(D⋯A)	(DHA)
3				
N–H⋯O4[a]	0.86	2.20	2.5928(1)	108
O–HA⋯O4[i]	0.85	1.89	2.7291(1)	171
O–HB⋯O2[ii]	0.85	1.92	2.7646(1)	175
O3–H3⋯O[iii]	0.82	1.75	2.5659(1)	171
O5–H5⋯O1[iv]	0.82	1.72	2.5342(1)	175
C2–H2A⋯O2[v]	0.96	2.50	3.3219(1)	144
C2–H2C⋯O3[vi]	0.96	2.51	3.1663(1)	126

(i) X, y, z; (ii) 1 − x, −1/2 + y, ½ − z; (iii) 1 − x, −y, 1 − z; (iv) ½ + x, y, ½ − z; (v) x, ½ − y, −1/2 + z; (vi) −1/2 + x, ½ − y, 1 − z

D–H⋯A	d(D–H)	d(H⋯A)	d(D⋯A)	(DHA)
4				
N–H⋯O2[a]	0.88	2.35	2.6862(1)	103
N–H⋯O2A[i]	0.88	2.19	3.0055(1)	153
O3A–H3A⋯O1B[ii]	0.84	1.72	2.5521(1)	170
NA–HA⋯O2[i]	0.88	2.10	2.9542(1)	164
NA–HA⋯O2A[a]	0.88	2.34	2.6848(1)	104
O3–H3⋯O1C[iii]	0.84	1.72	2.5497(1)	171
NB–HB⋯O2B[a]	0.88	2.38	2.6972(1)	102
NB–HB⋯O2C[ii]	0.88	2.08	2.9408(1)	165
O3B–H3B⋯O1A[iv]	0.84	1.72	2.5535(1)	172
O3C–H3C⋯O1[i]	0.84	1.69	2.5268(1)	172
NC–HC⋯O2C[a]	0.88	2.35	2.6913(1)	103
NC–HC⋯O2B[v]	0.88	2.15	2.9815(1)	158
C2–H2B⋯O2A[i]	0.98	2.48	3.2904(1)	140
C2–H2C⋯O2C[ii]	0.98	2.39	3.3114(1)	157
C4–H4A⋯O3[a]	0.99	2.55	2.8941(1)	100
C2C–H2CA⋯O2[v]	0.98	2.59	3.5379(1)	163
C2C–H2CB⋯O2B[v]	0.98	2.60	3.2454(1)	124
C2B–H2BB⋯O2C[ii]	0.98	2.48	3.2948(1)	140
C2A–H2AB⋯O2[i]	0.98	2.51	3.3590(1)	144

(i) x, y, z; (ii) 1 − x, −1/2 + y, ½ − z; (iii) 1 − x, ½ + y, ½ − z; (iv) −1 + x, y, z (v) −x, −1/2 + y, ½ − z

D–H⋯A	d(D–H)	d(H⋯A)	d(D⋯A)	(DHA)
5				
N–H⋯O3[i]	0.88	2.05	2.7972(1)	142
NA–HA⋯O3A[i]	0.88	2.18	2.9466(1)	146
C4A–H4AA⋯O1A[i]	0.99	2.44	3.3310(1)	150
O2–H2⋯O1A[ii]	0.94	1.72	2.6573(1)	175
O2A–H2A⋯O1[iii]	0.92	1.75	2.6583(1)	166
C4A–H4AA⋯O1A[i]	0.99	2.44	3.3297(1)	150
C3–H3⋯O3[a]	1.00	2.49	2.8753(1)	102
C21A–H21A⋯O4[iv]	0.95	2.48	3.4100(1)	165

(i) x, 1 + y, z; (ii) ½ − x, 1/2 + y, ½ − z; (iii) ½ − x, −1/2 + y, ½ − z; (iv) −1/2 + x, −1/2 + y, −1/2 + z

[a] Intramolecular interactions.

paid to the occurrence of the bifurcated H-bonding topology in the studied crystals.

The tendency of the oxygen atoms of the C=O and S of SH groups to act as acceptors of two H-bond interactions related to the NH/CH and SH/CH groups, respectively, as well as the hydrogen atom of CH to act as a donor of two H-bond interactions related to the SH/CH groups, is a specific feature of the supramolecular organization of the novel crystals, introducing a stronger cooperativity effect. An additional feature that arises from this work is that a wide variety of H-bonding supramolecular patterns result from the cyclopropyl moiety (Fig. S3†). Specifically, $_{cyclopropyl}$C–H⋯O$_{carbonyl}$, $_{cyclopropyl}$C–H⋯O$_{hydroxyl}$, $_{cyclopropyl}$C–H⋯O$_{H_2O}$, $_{cyclopropyl}$C–H⋯O$_{C–O–C}$, $_{cyclopropyl}$C–H⋯C$_{aryl}$, $_{aryl}$C–H⋯C$_{cyclopropyl}$ and $_{cyclopropyl}$C–H⋯C$_{cyclopropyl}$, $_{cyclopropyl}$C–H⋯N$_{arom}$, $_{cyclopropyl}$C–H⋯S, and $_{cyclopropyl}$C–H⋯F, interactions employed in the cyclopropyl-based synthons are specified (Table 3). The last three interactions, together with $_{cyclopropyl}$C–H⋯O$_{C–O–C}$, are observed only in the literature structures. The synthon denoted as B4$_{cyclopropyl}$, created by $_{cyclopropyl}$C–H⋯O$_{carbonyl}$ and C1$_{cyclopropyl}$, formed by an additional NH⋯O$_{carbonyl}$, is the most favorable cyclopropyl-based motif.

In summary, the heterosynthon called R$_2^1$(6), via N–H⋯O$_{carbonyl}$ and $_{aryl/cyclopropyl}$C–H⋯O$_{carbonyl}$ interactions, designated as C1/C1$_{cyclopropyl}$, is the most common cyclic motif in all the compounds derived from cyclopropyl-containing peptide-based compounds known thus far. All the identified graph-set notations (up to 20-membered motifs) are collected as a library in Table S6,† while all the cyclopropyl-based H-bonding patterns, at two graph-set theory levels, in **1–5**, are shown in Fig. S4–S8,† respectively.
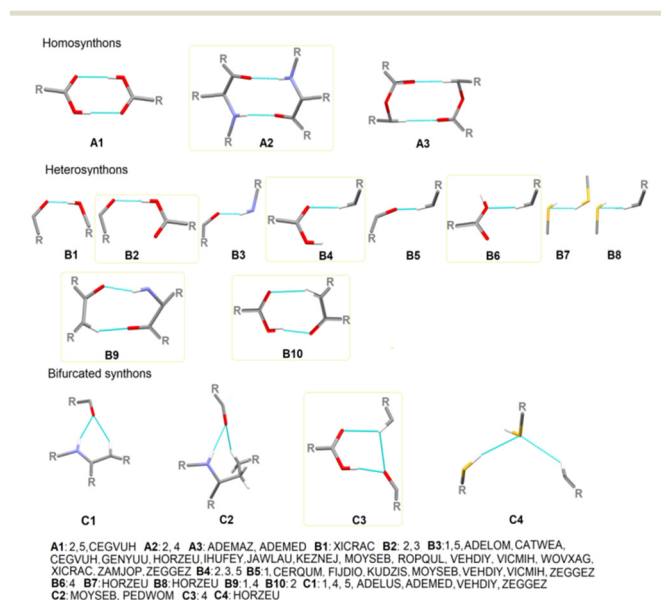

Fig. 1 Particular basic supramolecular H-bonding patterns identified in compounds **1–5** and those derived in CSD (new motifs are indicated by yellow frames).

Table 3 Summary of the contribution of particular interactions (and functional groups) to the formation of supramolecular cyclopropyl-based synthons in the newly synthesized compounds and those derived from CSD

Type of interaction	Occurrence	
cyclopropyl$C–H \cdots O_{carbonyl}$	2, 5	ADELOM, ADELUS, ADEMAZ, ADEMED, BUTCIE, CEGVUH, EDIWIZ, GENYUU, HILXIM, IHUFEY, JAWLAU, ROPQUL, VEHDIY, VETKEL, ZAMJEE, ZAMJOP
cyclopropyl$C–H \cdots O_{hydroxyl}$	2, 3, 5	CATWEA
cyclopropyl$C–H \cdots O_{H_2O}$	3	
cyclopropyl$C–H \cdots O_{C–O–C}$		ADEMAZ, PEDWOM
cyclopropyl$C–H \cdots C_{aryl}$	1, 4	
aryl$C–H \cdots C_{cyclopropyl}$	1, 5	
cyclopropyl$C–H \cdots C_{cyclopropyl}$	2, 4	
cyclopropyl$C–H \cdots N_{arom}$		CERQUM, GENYUU, PEDWOM, ZUQBIY
cyclopropyl$C–H \cdots S$		CERQUM
cyclopropyl$C–H \cdots F$		PEDWOM, WICMIH

Crystal packing of compound 1. Single-crystal X-ray structure analysis indicated that **1** crystallizes in an orthorhombic system, with the polar $Pna2_1$ space group and one molecule in its asymmetric unit. The self-assembled supramolecular architecture is governed by strong classical $O–H \cdots O$ and $N–H \cdots O$ H-bonds and is supported by weaker non-conventional $C–H \cdots O$ and $C–H \cdots C$ interactions linking molecules into diverse H-bonding synthons. Closer inspection indicated that at the first level of graph-set theory, two simple supramolecular chains, through the graph-set descriptor $C(4)$, are formed by $N–H \cdots O1_{carbonyl}$ (synthon B3, presented in Fig. 1) and $_{aryl}C2–H2A \cdots O1_{carbonyl}$ (synthon B5), respectively (Fig. 2), while at the second level, these H-bonds participate in the building of the cyclic motif denoted as an $R_2^1(6)$ ring pattern (synthon $C1_{cyclopropyl}$, presented in Fig. S2†). Another discernible feature is that the oxygen atom of the C=O group acts as a bifurcated acceptor to N–H and C–H donors (Fig. 2). In addition, $N–H \cdots O1_{carbonyl}$ together with the $_{aryl}C2–H2B \cdots O4_{carbonyl}$ interaction generates another simple dimer motif, designated as $R_2^2(9)$, (synthon $B9_{cyclopropyl}$). The fused heteromeric $R_2^1(6)$ and $R_2^2(9)$ motifs propagate alternately along the crystallographic *a*-direction, forming a ribbon. Interestingly, $R_2^1(6)$ and $R_2^2(9)$ are arranged in the form of a triple H-bonding motif (the three-point synthon). In the perpendicular plane, the cyclopropyl moieties connect molecules together into larger fused cyclic patterns (Table S6†).

Another feature worth considering is the long-range synthon Aufbau module (LSAM), a concept close to the cooperative effect, which is related to a stable packing motif constructed from different synthons,[149] and based on Kitaigorodskii's ideas on the Aufbau principle.[150] The LSAMs, so-called large synthons, consist of more than one type of inter-contact to summarize all the discovered H-bonding motifs controlling the packing of the molecules. In this context, in **1**, the lack of COOH groups in the molecule leads to the activation of peptide $N–H \cdots O$ bonds, which join molecules into a 1D structure along the *a*-direction and symmetry of the pc rod group (blue lines in Fig. 3). The chains are packed almost hexagonally, and the distortions are caused by secondary $C–H \cdots O$ interactions, which are marked as thin green lines.

Crystal packing of compound 2. The crystal of **2** belongs to the centrosymmetric triclinic $P\bar{1}$ space group. The molecules are arranged in the 'head-to-tail' type (Fig. 4). In the crystal lattice, the basic linear motifs, denoted as $C(7)$, formed by $_{hydroxyl}O3–H3 \cdots O1_{carbonyl}$ (synthon B2, see Fig. 1), $_{aryl}C2–H2A \cdots O2_{carbonyl}$ (synthon B4) and $_{cyclopropyl}C7–H7A \cdots O3_{hydroxyl}$ (synthon $B1_{cyclopropyl}$, see Fig. S2†), respectively, at the first level of the graph-set theory, are found. The first two chains are parallel to the *a*-axis, while the chain generated by the cyclopropyl-based interaction is prolonged along the *b*-direction. Remarkably, the combination of these H-bonds closes the rings, resulting in a basic cyclic homosynthon, featuring the graph-set notation as $R_2^2(8)$, built by $_{hydroxyl}O5–H5 \cdots O4_{carbonyl}$ H-bonds (synthon A1, Fig. 1), leading to the supramolecular linear chain propagated along the *cb*-plane. Perpendicularly, the
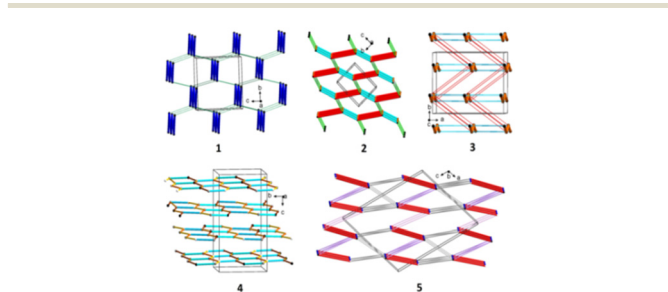

Fig. 2 Crystal packing in **1**, showing the intermolecular interactions and the supramolecular H-bonding synthons.

Fig. 3 Long-range synthon Aufbau modules, showing the H-bonding interactions in **1–5** (figure was prepared using Diamond v.4.6.6).[118]

heterosynthonic basic structural unit, represented by the same graph-set notation $R_2^2(8)$, is formed through the $_{hydroxyl}$O3–H3⋯O1$_{carbonyl}$ and $_{aryl}$C2–H2A⋯O2$_{carbonyl}$ interactions (synthon B10, Fig. 1), at the second graph set level of theory, propagated into another supramolecular linear chain extending along the crystallographic *a*-axis. Consequently, these tapes are interrelated into a 2-D planar sheet in the *ac*-plane, unveiling primary tetramer synthons, denoted as $R_4^4(26)$ and $R_4^3(24)$, between tapes. In another plane, cyclopropyl participates in the building of secondary H-bonding patterns. Further insight shows that the molecules are linked by 3-centre, bifurcated N–H⋯O and C–H⋯O interactions, leading to the very important $R_2^1(7)$ synthon (C4$_{cyclopropyl}$, presented in Fig. S2†).

Considering LSAMs, a supramolecular layer parallel to the crystallographic *bc*-plane is observed it is consistent with the $P\bar{1}$ space group symmetry, while its topology can be described as a 4-connected simple uninodal network, with a node being the centre of gravity of the molecule (black dot in Fig. 3), and edges in line with the observed H-bonds. Hence, the red lines represent a carboxylic dimer, cyan for the connections between the NH donor and the COOH acceptor, and the orange is for the COOH donor and peptide carbonyl atom. The network may be regarded as square planar with a {4·4} Schläfli symbol if the edges are indistinguishable. The thinner pink and green lines represent secondary C–H⋯O interactions, which lead to a 3D structure.

Crystal packing of compound 3. The crystal structure of **3** was determined in the orthorhombic, centrosymmetric *Pbca*

space group, with one symmetry-independent 2-(cyclopropylmethyl)-2-acetamidopropanedioic acid molecule and one crystallographically unique water molecule in the asymmetric unit. Herein, the adjacent molecules in the crystal lattice establish the wave-like architecture in the *ab*-plane (Fig. 5). The water molecule, as a bifurcated donor or bifurcated acceptor, acts as a bridge between the two main molecules that form the $C_2^2(8)$ motif *via* $_{aryl}$C4–H4A⋯O4$_{carbonyl}$ and $_{cyclopropyl}$C6–H6A⋯O5$_{hydroxyl}$ interactions. Consequently, a supramolecular zigzag chain is created. Moving forward, a similar supramolecular chain, denoted as $C_2^2(9)$, is built by the $_{H_2O}$O–HA⋯O4$_{carbonyl}$ and $_{cyclopropyl}$C6–H6B⋯O$_{H_2O}$ interactions, in which the cyclopropyl ring is employed. A perpendicular chain C(7) is formed through the $_{cyclopropyl}$C6–H6A⋯O5$_{carboxyl}$ interaction (synthon B1$_{cyclopropyl}$, Fig. S2†). By deeper exploration of the crystal lattice, diverse cyclic H-bonding patterns were also found, resulting in a 3D network. After further LSAMs analysis, the pc rod group symmetry describes the symmetry of the supramolecular chain structure, along the *c*-direction, formed by the H-bonds between the COOH group and the peptide carbonyl oxygen atom (thick orange lines in Fig. 3). The rectangular alignment of the main chains as viewed along the *c*-axis is more noteworthy rather than approximately hexagonal packing of rods. Responsible for this is the presence of crystalline water molecules. The presence of crystalline water molecules is responsible for this. In the figure, the water bridges are represented by thin red and cyan lines.

Crystal packing of compound 4. Compound **4** crystallizes in the monoclinic system, centrosymmetric P_12_1/c_1 space group,
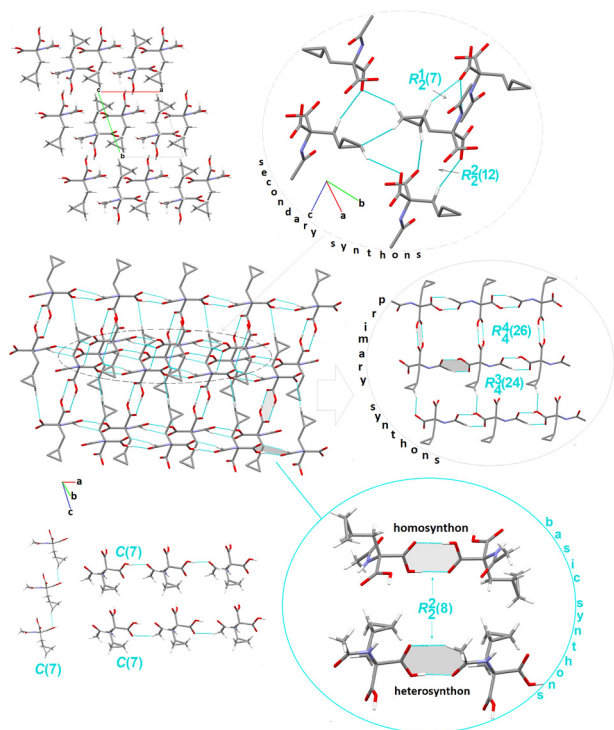

Fig. 4 Crystal packing in **2**, showing the intermolecular interactions and the H-bonding supramolecular synthons. H-atoms that are not engaged in the interactions are omitted for clarity.
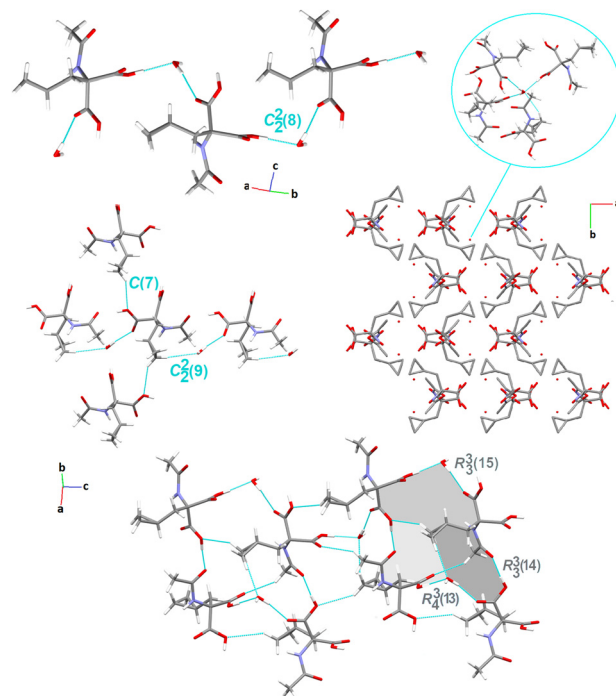

Fig. 5 Crystal packing in **3**, showing the intermolecular interactions and the H-bonding supramolecular synthons. H-atoms that are not engaged in the interactions are omitted for clarity.

with a surprisingly high number of crystallographically independent racemic Ac-b-cyclopropyl-(R,S)-Ala-OH moieties, $Z' = 16$. In this context, **4** provides exclusivity in comparison with the cyclopropyl-containing peptide-based structures deposited in the CSD. Notably, these compounds attract special attention for pharmaceutical applications.[151] Among the studied crystals, the supramolecular assembly of **4** (Fig. 6) is constructed and stabilized through the most diverse inter-contacts, *i.e.*, O···H/H···O, O···C/C···O, C···H/H···C, N···H/H···N, O···N/N···O, and O···O (see section below). Specifically, the $_{aryl}$C2A–H2C···O3A$_{hydroxyl}$ interaction links adjacent molecules into the sinusoidal supramolecular chain, denoted as C(7) (synthon B6, Fig. 1), which is parallel to the *a*-axis. O–H···O, N–H···O and C–H···O H-bonds participate in the construction of an interesting sheet consisting of fused cyclic two heterosynthons and one homosynthon, with the graph-set notation of $R_2^1(6)$, (synthon C1), $R_2^2(6)$ (synthon C3), and $R_2^2(10)$ (synthon A2). The stacking of the sheets is observed, providing an extra advantage for this structure. Alternatively, these tapes are interconnected by cyclopropyl-based interactions. Within the tapes, the H-bonding interactions are built in the mode of the repeated patterns of fused cyclic supramolecular H-bonding motifs.

From the LSAMs point of view, pseudo-centrosymmetric $R_2^2(10)$ dimers (light blue and cyan lines in Fig. 3) align alternately in the *ab*-plane and are further connected *via* topologically similar O–H···O bonds between COOH donors and peptide carbonyls (*i.e.*, each dimer is both a donor and an acceptor). Together, the above-mentioned interactions establish a honeycomb-like layer perpendicular to the *c*-direction. The development of a layer occurs by translational vectors only. Hence, the layer symmetry is given by the *p*1 layer group. Assuming that all the vertices and edges are unified, the Schläfli symbol of the 2D supramolecular unit is {6·3·3}. There are four layers per unit cell related by symmetry elements of the $P2_1/c$ space

symmetry group. The secondary weak C–H···O interactions are visible between the layers.

Crystal packing of compound 5. Compound **5** crystallizes in a monoclinic system, in the $I12_1$ space group, and its asymmetric unit is comprised of two independent Fmoc-b-cyclopropyl-(S)-Ala-OH molecules. They are connected through $_{hydroxyl}$O2A–H2A···O1$_{carbonyl}$ H-bonds into a centrosymmetric dimer. Consequently, the cyclic array $R_2^2(8)$, a robust and very popular synthon (synthon A1, Fig. 1), is formatted. This pattern is propagated into columns along the *b*-direction, linking the molecules into tetramers, which are denoted as $R_4^4(38)$ motifs (Fig. 7). Through a deeper exploration of the crystal structure, the $R_3^2(7)$ trimer, built by O–H···O and C–H···O H-bonds (synthon C8$_{cyclopropyl}$, Fig. S2†), unit is identified. This trimer is further fused to the mentioned earlier dimers, connecting tetramers and other cyclic motifs and creating a 2D layer. The parallel layers are connected by $_{cyclopropyl}$C6A–H6AB···O1A$_{carbonyl}$ interactions, creating a chain called C(7) (synthon B2$_{cyclopropyl}$, Fig. S2†). Interestingly, $R_3^2(7)$ and $R_2^2(8)$ are arranged in the four-point synthon. It should be noted that in contrast to all the other structures considered herein, **5** possesses the most intriguing feature, given that the electron-rich planar Fmoc ring system displays π-stacking behavior. Thus, H-bonding interactions are assisted by C–H···π and π···π interactions. These inter-contacts complete the final topology and stabilize the supramolecular assembly.

At the LSAMs level, the earlier described basic synthons, pseudo-centrosymmetric dimers $R_2^2(8)$ (red lines in Fig. 3, and black and white nodes signify two crystallographically independent molecules), are joined into a 1D ladder structure through the peptide N–H···O hydrogen bond along the *b*-direction. The motif has only translational symmetry. The numerous C–H···O (pink lines) and C–H···π (grey lines) interactions combine these ladders into a 3D structure.
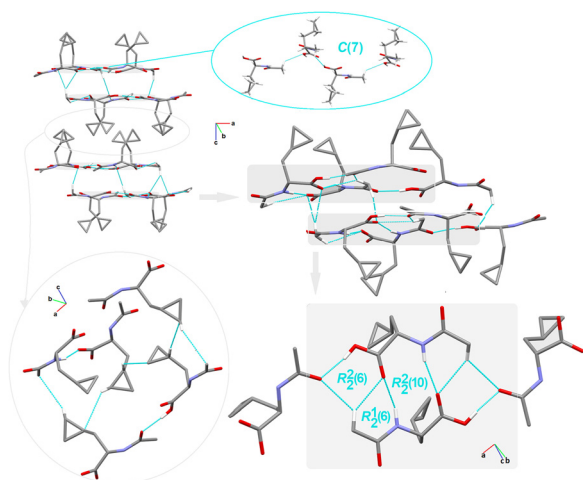

Fig. 6 Crystal packing in **4**, showing the intermolecular interactions and the H-bonding supramolecular synthons. H-atoms that are not engaged in the interactions are omitted for clarity.
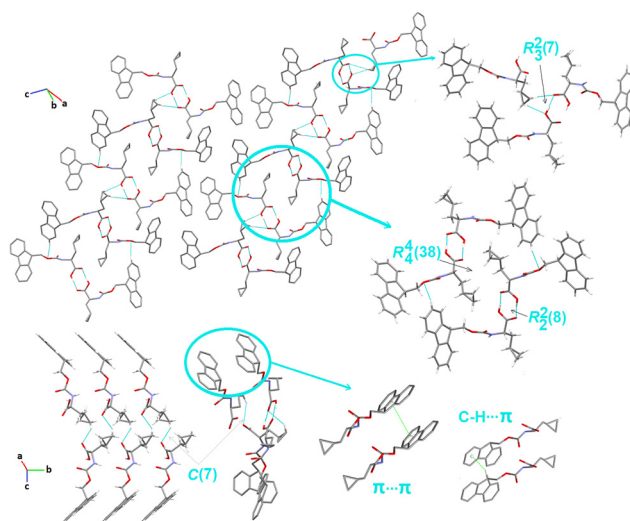

Fig. 7 Crystal packing in **5**, showing the intermolecular interactions and the H-bonding supramolecular synthons. H-atoms that are not engaged in the interactions are omitted for clarity.

3.2. Hirshfeld surface analysis

To fully elucidate the supramolecular preferences among the new crystals, the Hirshfeld surface (HS) methodology[103–107] was applied. The 3D HS maps with different properties (d_{norm}, d_e, d_i, electrostatic potential, shape index, curvedness, and fragment patch) of all the studied crystals are presented in Fig. S9.† The red-white-blue color scheme on the d_{norm}-mapped HSs is related to the inter-contacts shorter than, equal to, and longer than the sum of the vdW radii, respectively. The existence of bright red spots denotes the dominant close interactions and identifies the strongest H-bonds, such as O···H and N···H, which are the O-atoms of the carboxy groups, N-atoms of the amino groups, and H-atoms of the hydroxy/amino groups. The light blue smaller spots on the surface signify the weaker C···H and H···H inter-contacts. In **5**, the shape index and the curvedness properties are helpful in the recognition of π-stacking arrangement *via* the presence of adjacent blue and red triangles (bow-tie pattern) and large green flat areas (brown circle in Fig. 8), respectively. The blue triangles correspond to the convex regions (the atoms of the molecule inside the surface) and the π-hole (the π-stacked molecule above it). This is consistent with the FP, which presents the contribution of the C···C interactions (the triangle near $d_e = d_i \approx 1.8$ Å refers to the characteristic of π–π interactions). In the other compounds, π-stacking contacts are not observed. The circle in pink represents π-stacking from an aromatic proton outside the surface (red bulging area) around the CH_2 moiety and the complementary proton inside the surface (blue hollow spot), indicating C–H···π interaction. As noted in Table S4,† the shortest face-to-face π···π contact was Cg(2)[C11–C12–C17–C18–C23]···Cg(3)[C12–C13–C14–C15–C16–C17] with an interaction distance of 3.9579(1) Å, while the

T-shaped C–H···π was C10A H10B···Cg(9)[C11A–C12A–C17A–C18A–C23A] with 2.4488(1) Å (Table S5†). The fragment patch on the HSs characterize the coordination environment of the molecule in the crystal. The coordination number is determined by the curvedness of the HS. The extensive green flat areas of the HS have low values, whereas the sharp areas have high values of curvedness, resulting in the division of the surface into colour patches related to interactions among the nearest-neighbouring molecules. The collection of the color patches specifies the different independent species in the title structure.

The formation of H-bonds in the crystal molecules is elegantly driven by electrostatic interactions. The electrostatic potential (EP), mapped on the HS, reveals negative (red area) and positive (blue region) potentials, indicating the H-bond acceptor and donor sites, respectively. Thus, the EP maps provide direct insight into the sensitivity of a molecule toward chemical reactivity, which can be helpful in the identification of '3D pharmacophore points', visualizing the donor and acceptor sites.[42] To compare the total share of strong and weak interactions in the formation of synthons, we present the differences between the most extreme **2** and **5** crystals using fingerprint plots and EP maps (Fig. 8). In the latter, 24% inter-contacts is the sum of contributions of C···H/H···C (22.5%) and C···C (1.5%), while in **1**, only 2.5% of all the interactions, derived from the C···H/H···C, participate in a set of H-bonding donors and acceptors. Nevertheless, in both crystals, weak cyclopropyl-based interactions are employed in the formation of the main synthons that govern the self-assemblies, such as $C(7)$, denoted as $B1_{cyclopropyl}$ synthon, in **2** and $R_3^2(7)$, called $C8_{cyclopropyl}$, in **5**, visible in the EP mapped on the HSs. It should be noted that the electron-rich sites are located in the semi-transparent EP, mapped on the HSs, around the oxygen atoms (and the π-system of the Fmoc group). The electrostatic complementarities of the touching surface patches in the neighbouring molecules for all the studied crystals are presented in Fig. S9.†

Precisely, an analysis of all the fingerprints (FPs), which is useful in the comparison of the supramolecular features of all novel solids in terms of clear quantitative identification of each type of inter-contact, is necessary. The overall FPs are presented in Fig. 9, which are delineated into the corresponding types of interactions, such as H···H, O···H/H···O and C···H/H···C for compounds **1–3**, H···H, O···H/H···O, C···H/H···C, C···O/O···C, N···H/H···N, O···N/N···O and O···O for compound **4** and H···H, O···H/H···O, C···H/H···C, C···O/O···C and C···C for compound **5** in Fig. S10.† The relative percentage contributions of the various close inter-contacts, both external and internal in the terms of diverse atoms, to the HS area of the compounds are demonstrated in Fig. 9 (Table S7†), where subtle differences are clearly highlighted. In particular, subtle H···H (~50% in **2** and **3**, 60% in **5**, and 70% in **1** and **4**) are the most significant interactions in all the analysed crystals due to the numerous H-atoms on the molecular surface where diverse vdW
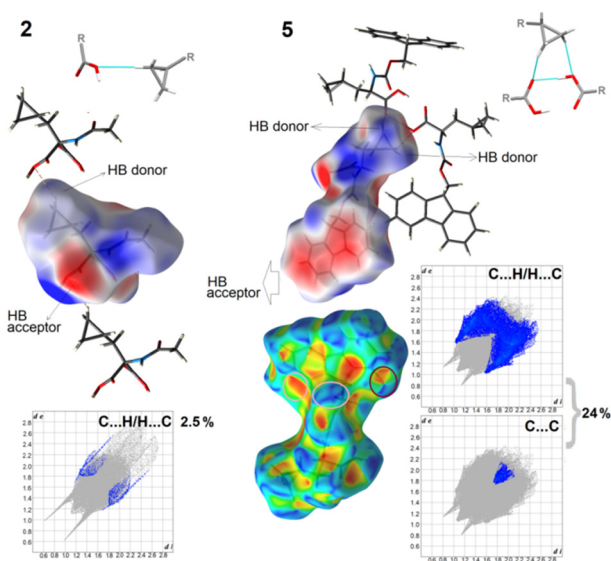

Fig. 8 Electrostatic potential maps, showing selected supramolecular synthons, and delineated fingerprint plots into weak interactions in **2** and **5**.
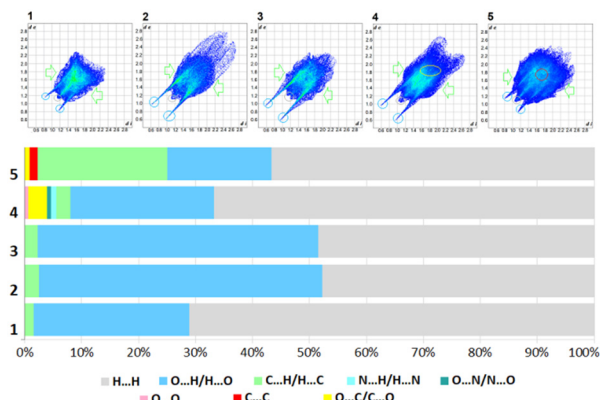
Fig. 9 2D fingerprint plots and percentage contributions of inter-contacts to the Hirshfeld surface in structures **1**–**5** (regions of particular interactions are indicated by the ovals in the FPs).

contacts are formed. Strong O⋯H/H⋯O H-bonds are the other major contributors to the HS, especially in the case of **2** and **3**, where they account for ∼50%, due to the presence of additional carboxylic groups in the structure, while in other crystals are at the level of ∼20–25% of all the interactions. Alternatively, in **5**, weak C⋯H/H⋯C inter-contacts have a considerable coverage (∼23%) of the total surface, while in the other crystals, their contribution is less than 3%. In contrast, the share of O⋯H/H⋯O H-bonds is the lowest among the crystal structures. Moreover, O⋯C/C⋯O contacts are observed in **4** (3.3%) and **5** (∼1%), while C⋯C only in **5** (1.5%) due to the presence of the fluorenyl group in this structure. Furthermore, N⋯H/H⋯N, O⋯N/N⋯O and O⋯O inter-contacts are present in **4**, but the factors are only ∼1% (Table S7†). Thus, in **4**, the most complex molecular surface with the greatest diversity of intercontacts is observed, following the order of H⋯H > O⋯H/H⋯O > O⋯C/C⋯O > C⋯H/H⋯C > N⋯H/H⋯N > O⋯N/N⋯O and O⋯O.

To better understanding the propensity for the privileged and disfavoured interactions between a pair of chemical species in a crystal structure, the enrichment ratios (ER),[152] based on the HS analysis, were determined for all the studied compounds and presented in Table S8.† In this regard, the inter-contacts with high propensity to construct stable supramolecular architecture are as follows: O⋯H/H⋯O and C⋯H/H⋯C in **1**, **2**, **3**, **5**; O⋯H/H⋯O, O⋯C/C⋯O, and O⋯N/N⋯O in **4**. The thorough inspection revealed that H⋯H contacts are more favoured in **4**, **1**, and **5** (ER = 1.01, 0.97, and 0.96, respectively) than in others (ER = 0.88 in **2** and 0.89 in **3**), which is consistent with the HS calculations. The opposite trend was observed for the O⋯H/H⋯O and C⋯H/H⋯C inter-contacts, where in **2** and **3**, the ER is 1.35, while it is 1.25 for O⋯H/H⋯O and 1.12 for C⋯H/H⋯C in **5**, 1.17 in **1**, 1.02 for O⋯H/H⋯O and only 0.53 for C⋯H/H⋯C in **4**. It is also important to note that in **4**, O⋯C/C⋯O and O⋯N/N⋯O are greatly enriched with ER = 3.75 and 2.92, respectively, due to the relatively high value of their proportion on the molecular surface. In **5**, C⋯C are slightly favoured (ER = 0.87).

Finally, to gain a complete view on the landscape of interactions, their relative strength and topologies in the studied crystals, we systematically compared the energy frameworks (EFs). In this regard, the crystal structures were studied by comparing their pairwise interaction energies. The molecular pairs are uniquely color-coded, as shown in Fig. S11,† while the energies of the inter-contacts are summarized in Table S9.† The 3D topology of the crystal packing is visualized via EFs for **1**–**5** in Fig. S12† to better understand the supramolecular rearrangement in all the crystal lattice directions. At first glance, some differences are noticeable. Crystal **5** possesses a unique architecture of molecular interaction topology. Specifically, the herringbone energy framework propagates along the *a*-direction, comprising molecules linked by weak interactions. The width of the cylinders correlates with the relative strength of the energy between the molecules (a greater radius indicates more substantial and prominent interactions). However, the diversity in the dimensions of these cylinders, *i.e.*, pillars, columns, and crossbars, in the supramolecular architecture of the energy frameworks cannot be overlooked. The nature of the specific interactions is denoted by a red–green–blue colour scheme, signifying the electrostatic, dispersive, and total energy, respectively. A significant contribution of the electrostatic energy term, related to the strong classical interactions, is noticeable in **2** (the total electrostatic energy is −252.6 kJ mol⁻¹), while in **1** (the total dispersive energy is −147.3 kJ mol⁻¹), **4** (−93.1 kJ mol⁻¹) and **5** (−322.9 kJ mol⁻¹), where the dispersion terms responsible for weak interactions are favorable in terms of stabilization of the crystal lattice. In **3**, the difference between the electrostatic (−148.1 kJ mol⁻¹) and dispersion (−163.1 kJ mol⁻¹) terms is not considerable. Indeed, a delicate balance is observed between the strong and weak interactions, with a slightly dominant dispersion component. In comparison, the polarization energy contributed slightly to the total energy of **1** (−21.2 kJ mol⁻¹) and **4** (−14 kJ mol⁻¹). The data in Table S9† indicate that the total energies follow the order of **5** (−327.3 kcal mol⁻¹) > **2** (−265.6 kcal mol⁻¹) > **3** (−175 kcal mol⁻¹) > **1** (−140.7 kcal mol⁻¹) > **4** (−94.3 kcal mol⁻¹).

3.3. Quantum-chemical calculations: cyclopropyl

3.3.1. Cyclopropyl-based interactions. These interactions, as investigated in suitable dimers of the molecules under study by QTAIM analysis, revealed that the interactions between two cyclopropyl rings, the interactions of the cyclopropyl ring with non-cyclopropyl atoms of the other molecule (Fig. 10) and the inter-contacts between the cyclopropyl carbon atom and the hydrogen atom of the other molecule, are possible but are very weak for the bond paths, as shown in Fig. S13.†

3.3.2. Chemical nature of cyclopropyl ring in 1–5. To check the potential of the cyclopropyl ring in the new compounds to create π-based synthons, we focused on the influence of strain in the cyclopropyl ring (Scheme S1†). In addition, to

the NBO treatment,[153] we alternatively used QTAIM treatment to evaluate the molecular strain at the individual active sites of the molecule. In particular, we concentrated on the common parts of molecules **1**, **2** (**3**), **4**, and **5** (containing both cyclopropyl and methylene groups) and their comparison with cyclopropane, see Fig. 11 and S14–S17 in the ESI† for optimized geometries of C_3H_6 and analyzed molecules and Tables 4 and S10† for their relevant bond lengths and angles. The lengths of the C–C bonds in the cyclopropyl ring are comparable to the neighbouring C5–C4 bond. The aliphatic C4–C3 bond is significantly longer. The C–H bonds to the secondary C6 and C7 atoms are shorter than to the tertiary C5 atoms. Except for compound **5**, the aliphatic C5–H5 bonds are even longer. The effect of the R_i substituent on the C–C and C–H bonds at the cyclopropyl ring disappeared and the same was observed for the C–C, H–C–H, and H–C–C angles (Table S10†). The C5–C4 bond angles with the aliphatic C3 atom are significantly lower than that with the cyclopropyl C atoms. The H4–C4–H4A angles are significantly lower than the analogous H–C–H angles related to the cyclopropyl ring and similar relations hold for the analogous H–C–C angles. The natural charges (Table S11†) of the secondary C6 and C7 atoms in cyclopropyl are comparable to the aliphatic C4 atoms, whereas the charges of the tertiary C5 atoms are much less negative. The positive charges of all the H atoms on cyclopropyl are nearly equal. The charges of the H4 atoms (except compound **5**) are higher and affected by R_i substituents. The cyclopropyl C–C bonds in the analyzed compounds are weaker than in C_3H_6 and do not depend on the substituents (Table S12†). The bond strengths decrease in the sequence of C5–C4 > C6–C7 > C6–C5 ~ C7–C5 > C4–C3, which is in agreement with the corresponding bond lengths (Table 4), *i.e.*, some bond strength change can be observed. The C–H bond strengths at cyclopropyl do not depend on the substituents. The natural sp^n hybrid orbitals at the cyclopropyl carbons (Table 5) contain an increased p electron contribution ($n > 3.3$), especially at the C5 atoms ($n > 3.5$) on account of the decreased p contribution in the C5–C4 bonding ($n \sim 2.2$). The aliphatic C4 and C3 atoms also exhibit a lower p contribution in the C–C bonds ($n < 2.8$). Reverse trends of carbon p contributions were observed in the C–H bonds, which decreased in the order of C4–H4 > C5–H5 > C6–H6 ~ C7–H7. The R_i substituent effects disappeared. The
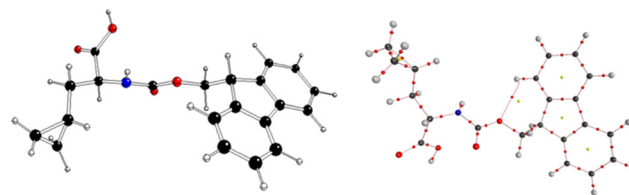

Fig. 11 On the left: M06/6-311++G(d,p) optimized structure of compound **5** (C – black, H – white, O – red, and N – blue). On the right: molecular graph of compound **5** (C – black, H – grey, O – red, N – blue, bond critical points – small red, and ring critical points – yellow).

deviations in the natural hybrid orbitals from the line connecting the bonded atoms in the cyclopropyl ring (Table S13†) are approximately 23°. Their dependence on the R_i substituents is very small. In this way, the obtained 'banana' bonds are bent at the carbon atoms by 107° (see Table S14†). As mentioned above (Table 5), this decrease in angle is related to the greater contribution of the p-electron to the natural hybrid orbitals (the p orbitals are mutually perpendicular), and thus minimizes the molecular strain.

The σ–π* and π–σ* interactions between the C–C bonds in the cyclopropyl ring and π-type orbitals in the rest of the molecule were found in compound **5** only (Table 6). The stabilization energies related to the carbonyl or aromatic π orbitals and aromatic π* orbitals are relatively low. Interactions were also found between the aromatic π* orbitals and the cyclopropyl σ* orbitals. The QTAIM molecular graphs of the systems under study are presented in Fig. 11 and S18–S21.† The additional molecular paths between the cyclopropyl hydrogens and carboxyl oxygen atoms in compounds **2** and **1** increase the differences in the cyclopropyl group (see below). The QTAIM charges of all the relevant H and C atoms are nearly equal to zero, unlike the NBO treatment (Table S11†), except for the positive C3 atomic charges, which depend on the R_i substituents (Table S15†). The atomic volumes (Table S16†) of the secondary C6 and C7 atoms are significantly higher than that of the tertiary C5 atoms. The aliphatic secondary C4 atoms have even slightly lower volumes. The significantly higher volumes of C6 and C7 atoms with nearly equal charges with C5 atoms reflect the
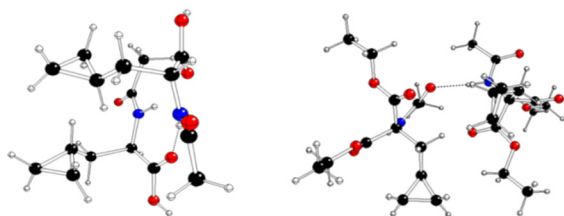

Fig. 10 On the left: M06/6-311++G(d,p) optimized structure of **4** dimer (C – black, H – white, O – red, and N – blue). On the right: M06/6-311++G(d,p) optimized structure of the **1** dimer (C – black, H – white, O – red, and N – blue).

Table 4 Relevant bond lengths (in Å) of the optimized structures under study (see Scheme S1† for atom notation)

Bond	C_3H_6	1	2	4	5
C6–C5	1.496	1.494	1.502	1.494	1.496
C7–C5	1.496	1.502	1.495	1.502	1.497
C6–C7	1.496	1.498	1.498	1.499	1.499
C5–C4	—	1.502	1.502	1.503	1.502
C4–C3	—	1.536	1.536	1.535	1.527
C6–H6	1.085(2×)	1.086	1.085	1.084	1.084
		1.084	1.086	1.086	1.086
C7–H7	1.085(2×)	1.087	1.084	1.086	1.087
		1.085	1.086	1.085	1.084
C5–H5	1.085(2×)	1.089	1.088	1.088	1.088
C4–H4	—	1.096(2×)	1.096(2×)	1.098	1.087
				1.096	1.084

Table 5 Relevant p electron contributions n in sp^n hybrids in individual bonds in the systems under study (see Scheme S1† for atom notation)

Bond	Atom	C_3H_6	1	2	4	5
C6–C5	C6	3.42	3.33	3.35	3.33	3.34
	C5	3.42	3.58	3.63	3.58	3.56
C7–C5	C7	3.42	3.34	3.34	3.33	3.36
	C5	3.42	3.65	3.59	3.62	3.64
C6–C7	C6	3.42	3.52	3.52	3.51	3.51
	C7	3.42	3.53	3.51	3.54	3.53
C5–C4	C5	—	2.20	2.21	2.21	2.24
	C4	—	2.44	2.43	2.42	2.38
C4–C3	C4	—	2.76	2.78	2.77	2.72
	C3	—	2.48	2.45	2.41	2.50
C6–H6	C6	2.65(2×)	2.66	2.63	2.67	2.64
			2.64	2.66	2.64	2.66
C7–H7	C7	2.65(2×)	2.66	2.64	2.66	2.65
			2.64	2.66	2.63	2.62
C5–H5	C5	2.65(2×)	2.94	2.93	2.93	2.89
C4–H4	C4	—	3.49	3.51	3.54	3.61
			3.51	3.49	3.48	3.55

higher chemical reactivity[102] of these cyclopropyl carbons. The BCP electron densities (Table S17†) indicate that the C–C bonds in cyclopropyl are comparable with the aliphatic C4–C3 bonds, whereas the C5–C4 bonds are stronger. The BCP Laplacians of the electron density (Table S18†) of the cyclopropyl C–C bonds are significantly less negative than the aliphatic ones. The BCP Laplacians of the electron density of all the C–H bonds are nearly equal and are significantly more negative than that of the C–C bonds. The extra high BCP ellipticities of the cyclopropyl C–C bonds (Table S19†) indicate a very high mechanical strain, which is slightly increased for weaker bonds (comparison shown in Table S17†). The aliphatic C5–C4 and C4–C3 bonds exhibit approximately one-order lower BCP ellipticities, *i.e.*, pure σ bonding with only slight mechanical strain. The C–C-BCP angles in cyclopropyl (Table S20†) are nearly halved compared to the natural hybrid orbital deviations from the C–C lines (Table 4). This can be explained by the curvatures of the 'banana' bonds given that the hybrid orbital deviations are evaluated directly at the carbon atoms and the corresponding BCPs are in the middle of these bonds.

Consequently, the BCP-C-BCP angles (Table S20†) are lower than the bond bending at the cyclopropyl carbons (Table S14†).

3.4. Biological screening

3.4.1. Bio-activity and ADMET profile. *In silico* prediction of the ADMET (absorption, distribution, metabolism, excretion, and toxicity)[109,110] profile revealed the potential ability of the novel compounds as therapeutic agents. The bioavailability radars, as shown in Fig. S22,† present very satisfactory drug-likeness, which are related to their physicochemical properties (Table S21†), while BOILED-egg (Brain Or Intestinal EstimateD permeation) diagrams show good absorption parameters and the possible blood–brain barrier permeability of **5** (Fig. S23†). Moreover, the probability maps (Fig. S24†),[112] obtained *via* the pred-hERG web tool, reveal the absence of cardiotoxicity in all the compounds. Notably, lipophilicity is a key property in the physicochemical characterization of bioactive substances given that it is strongly related to the ability of compounds to cross cell membranes and to interact with biological targets. It is affected by the chemical structure of the drug and the presence or absence of ionizable groups. In the case of ionizable compounds, the acid–base dissociation constant (pK_a) of a drug is becoming a key parameter influencing lipophilicity and many biopharmaceutical characteristics.[154] Log D is a distribution coefficient widely used to measure the lipophilicity of ionizable compounds, where the partition is a function of the pH. For non-ionizable compounds, log P = log D in the full pH range, whereas for ionizable compounds, log D takes into account the partition of both ionized and non-ionized forms. Log D is convenient for practical measurements, given that it takes into account solution pH, which is important for the analysis of the drug candidate properties in various biologic media with different pH values. In this context and at this juncture, we describe the results of the detailed experimental study of **5**, the most controversial based on the *in silico* parameters among novel compounds. In particular, the log $P_{oct/w}$ calculated using the SwissADME

Table 6 Second-order perturbation theory analysis of cyclopropyl C–C bond interactions with π-type bonds/lone electron pairs in compound 5

Type of interaction	Donor orbital population	Stabilization energy [kcal mol^{-1}]
$\pi(C{=}O)_{R3} \rightarrow \sigma^*(C6{-}C7)$	1.989	13.90
$\pi(C{=}O)_{R2} \rightarrow \sigma^*(C6{-}C7)$	1.995	0.58
$\pi(C{-}C)_{arom\text{-}sideR3} \rightarrow \sigma^*(C6{-}C7)$	1.662	9.00
$\sigma(C7{-}C5) \rightarrow \pi^*(C{-}C)_{arom\text{-}nearR3}$	1.952	0.59
$\sigma(C7{-}C5) \rightarrow \pi^*(C{-}C)_{arom\text{-}sideR3}$	1.952	3.51
$\sigma(C6{-}C7) \rightarrow \pi^*(C{-}C)_{arom\text{-}distR3}$	1.958	1.63
$\sigma(C6{-}C7) \rightarrow \pi^*(C{-}C)_{arom\text{-}nearR3}$	1.958	0.56
$\sigma(C6{-}C7) \rightarrow \pi^*(C{-}C)_{arom\text{-}distR3}$	1.958	2.60
$n_\pi(O)_{esterR3} - \sigma^*(C7{-}C5)$	1.820	78.25
$n_\pi(O)_{C{=}OR3} \rightarrow \sigma^*(C7{-}C5)$	1.830	198.74
$n_\pi(O)_{OHR2} \rightarrow \sigma^*(C7{-}C5)$	1.822	1292.47
$n_\pi(N)_{R3} \rightarrow \sigma^*(C7{-}C5)$	1.770	77.38
$\pi^*(C{-}C)_{arom\text{-}distR3} \rightarrow \sigma^*(C6{-}C7)$	0.370	22.19
$\pi^*(C{-}C)_{arom\text{-}sideR3} \rightarrow \sigma^*(C6{-}C7)$	0.343	1.63

software varies in the range of 2.76–5.99 with an average value of 3.84 (Fig. S25†). In this computational approach, the lipophilicity was calculated for the neutral form of **5** only, while the methodology used does not consider the fact that compound **5** is an ionizable molecule and the parameter defining the lipophilicity, more precisely, id $\log D$. The experimental pK_a for **5** is 3.60 and $\log P$ measured as a function of pH is 3.47 at pH 1 (stomach pH) when the compound is not ionized, whereas at higher pH such as 7.4 (blood pH), the lipophilicity is much lower and amounts to $\log D = -0.33$. This may obviously affect the bioavailability of the compound, depending on the route of administration. Therefore, in future considerations regarding the lipophilicity and bioavailability of compounds **1–5** in the context of a possible route of administration, the instability of the cyclopropyl ring at very low pH should also be considered.

Furthermore, we checked *via* the SwissTargetPrediction program,[155] that compounds **2–4** are potentially active toward protease inhibitor, enzyme, nuclear receptor, kinase, and membrane receptor, compound **1** shows activity toward protease, enzyme, family A G protein-coupled receptor, nuclear receptor, isomerase, kinase, writer and voltage-gated ion channel, while **5** shows activity toward protease, enzyme, family A G protein-coupled receptor, cytochrome P450, phosphatase and oxidoreductase (Fig. S26†). The bioactivity scores, 'a measure of a molecule's ability to interact with receptors', were predicted using the Molinspiration software.[156] In addition, the prediction of tumor (and non-tumor) cell line cytotoxicity was calculated using the CLC-pred website tool, which is based on the relationship between structure-cell line cytotoxicity *via* the PASS procedure.[113] Compound **2** (and **3**) exhibited cytotoxicity against prostate carcinoma tumor cell lines, with a Pa value of greater than 0.5, indicating a high probability of action. This is a promising finding in the face of the increasing heterogeneity of prostate cancer and the constant need for new-generation safe and effective therapeutic agents and on-going research in this field. Notably, this fatal disease (the second-leading cause of cancer death for men) remains incurable despite the many recent advances in therapies.[157]

3.4.2. Molecular docking analysis. Androgen hormones and their executor androgen receptors, including the human androgen receptor (hAR), are known to regulate crucial cellular functions that are involved in the initiation and progression of prostate cancer (PCa).[158] Therefore, we studied the binding affinity of promising active agent **2** and hAR. *In silico* calculations were carried out with the AutoDock Vina program using the crystal structure of hAR (PDB: 1E3G) retrieved from the Protein Data Bank and docked with **2** as the ligand (Fig. 12). For validation of the docking protocol and the subsequent analysis of the docking results, two prominent drugs, *i.e.*, metribolone (R1881) and flutamide, were docked as control ligands (for more details, see ESI†). The results showed that the maximum docking score of **2** in hAR was -5.9 kcal mol^{-1}, which showed its relatively high potency to form stable complexes with hAR even when

compared to the employed powerful active agents R1881 (-8.0 kcal mol^{-1}) and flutamide (-7.9 kcal mol^{-1}). Fig. 12 shows the docking results depicting the intermolecular interactions between **2** and the amino acids on hAR. Molecular docking revealed that the critical interacting amino acids at the active site of hAR included Asn705 and Thr877. These residues formed conventional hydrogen bonds with the carboxylic acid moiety of **2** with distances in the range of 1.9–2.3 Å. Other beneficial ligand–receptor interactions potentially responsible for stabilizing the hAR-2 complex include the alkyl-type interactions observed between the carbon atoms of the ligand cyclopropane ring and neighboring methylene group, as well as the aliphatic amino acids of the receptor (*i.e.*, Leu704, Met742, and Met745), respectively. In addition, Phe764 accommodated in the substrate-binding pocket exhibited π-alkyl interactions with the cyclopropane ring, while Trp741, Ile899, Leu880, Phe876, Met895, Phe891, Leu873, and Met780 were involved in vdW interactions with the ligand molecule. Furthermore, the computational data demonstrated that the incorporated cyclopropyl ring acts as a 'hydrophobic anchor', which allows the ligand molecule to be accommodated in the binding pocket of the enzyme in such a position that its polar functional groups are directed closer toward the H-bonding-capable carboxylic acid or hydroxy moieties of the Asn705 and Thr877 residues, respectively.

Overall, the results of the *in silico* studies showed that **2** is a promising candidate for further evaluation for prostate cancer prevention or management.
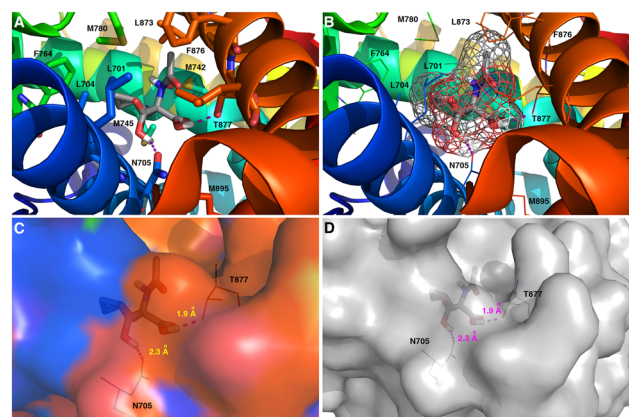

Fig. 12 *In silico* study of **2** binding to the human androgen receptor (hAR, PDB code: 1E3G). (A and B) Interactions between **2** and hAR in the substrate-binding pocket. (C and D) Surface model of the docking site showing **2** fits the pocket of hAR. The most significant amino acid residues contributing to the stabilization of the ligand molecules are shown in the stick (A) or line (B) representations, respectively. (B) Electron density map of ligand **2** corresponds to the $F_o - F_c$ and is shown in the meshing representation. The carbon atoms are colored gray, the nitrogen atoms with blue color, the oxygen atoms red, and the polar hydrogen atoms white. The formation of potential intermolecular hydrogen bonds is represented by dashed magenta lines. The mutual distances between the amino acid residues and the respective ligand atoms are given in Å (see C and D).

4. Conclusions

Herein, we reported the synthesis of novel cyclopropyl-containing compounds, namely, diethyl 2-acetamido-2-(cyclopropylmethyl)malonate (**1**), 2-(cyclopropylmethyl)-2-acetamidopropanedioic acid (**2**) [Ac-b-cyclopropyl-(R,S)-Ala-OH], 2-(cyclopropylmethyl)-2-acetamidopropanedioic acid hydrate (**3**), 2-acetamido-3-cyclopropylpropanoic acid (**4**), and (2S)-2-[cyclopropyl(9H-fluoren-9-ylmethoxycarbonyl)amino] propanoic acid (**5**) [Fmoc-b-cyclopropyl-(S)-Ala-OH]. Based on the in-depth supramolecular analysis, the influence of cyclopropyl in the construction of impressive structural landscapes at different levels of supramolecular architecture was unveiled. New H-bonding cyclopropyl synthons were identified and systematized in terms of all the cyclopropyl-containing peptide-derived compounds known thus far, building a library, which can be used for planning future studies on more effective, next-generation drugs of diverse categories due to the versatility of the analysed synthon functionalities. The Hirshfeld surface analysis revealed the intricacies of the H⋯H, H⋯O/H⋯O, and C⋯H/H⋯C interactions in **1**–**5**, H⋯N/N⋯H, O⋯N/N⋯O, and O⋯O in **4**, O⋯C/C⋯O in **4** and C⋯C related to π⋯π stacking forces and C–H⋯π inter-contact that steer the self-assembly of **5**, and provided a deeper understanding of how cyclopropyl stabilizes the crystal packing. The relative contributions of the inter-contacts and enrichment ratios establish the cyclopropyl synthon as an important contributor, acting both as an H-bonding donor and acceptor, mainly *via* C–H⋯O interactions. Although weak cyclopropyl-based interactions play a secondary role, they introduce a stronger cooperativity effect. Electrostatic potential maps helped us to correlate the weak interactions with the electrostatic complementarity between them. The energy frameworks demarcated the dominant contribution of the electrostatic energy term (related to the strong classical interactions) in **2**, while that in **1**, **4**, and **5** was the dispersion terms (weak interactions). In **3**, the difference between both terms is not considerable. NBO and QTAIM treatments explained the relation between the p electron contributions in the sp^n hybrid orbitals in the carbon atoms and the mechanical strain in the corresponding bonds. The σ/σ* natural C–C bonds in the cyclopropyl rings require the presence of an aromatic substituent, although very distant, to allow their low-energy stabilizing interaction with π*/π bonds not only within the aromatic rings but also at the C=O groups outside the aromatic part. Extra-high stabilizing energies correspond to the interaction of non-bonding π-type lone pairs at the O or N atoms with σ* natural C–C bonds in the cyclopropyl rings. In addition, the novel compounds have attractive *in silico* pharmacokinetic parameters. The molecular docking study revealed that cyclopropyl is engaged in the stabilization of the bio-complex *via* C–H⋯C$_{cyclopropyl}$ and C–H$_{cyclopropyl}$⋯π interactions with the key amino acid residues inside the active pocket of the human androgen receptor. Cyclopropyl acts as a 'hydrophobic anchor', which allows the ligand molecule to be accommodated in the binding pocket of the enzyme. Notably, compound **2** (and **3**) shows a significant docking score with effective binding affinity, and thus is a promising candidate for prostate cancer prevention or management.

Finally, we demonstrated that cyclopropyl plays an essential role in the (bio)supramolecular architecture. We hope that the findings reported herein will stimulate further investigations on new types of cyclopropyl synthons and will be useful for researchers working not only in the field of crystal engineering and supramolecular chemistry but also in peptide(ligand)–protein(target) interactions.

Author contributions

Conflicts of interest

There are no conflicts to declare.

Acknowledgements

References

1 K. B. Wiberg, *Angew. Chem., Int. Ed. Engl.*, 1986, **25**, 312–322.

2 E. Kochanski and J. M. Lehn, *Theor. Chim. Acta*, 1969, **14**, 281–304.

3 F. H. Allen, O. Kennard, D. G. Watson, L. Brammer, A. G. Orpen and R. Taylor, *J. Chem. Soc., Perkin Trans. 2*, 1987, S1–S19.

4 C. A. Coulson and T. H. Googwin, *J. Chem. Soc.*, 1963, 3161.

5 A. Galano, J. R. Alvarez-Idaboy and A. Vivier-Bunge, *Theor. Chem. Acc.*, 2007, **118**, 597–606.

6 M. E. Jason and J. A. Ibers, *J. Am. Chem. Soc.*, 1977, **99**, 6012–6021.

7 T. S. Cameron, A. Linden and K. Jochem, *Acta Crystallogr., Sect. C: Cryst. Struct. Commun.*, 1990, **46**, 2110–2115.

8 A. de Meijere, *Angew. Chem., Int. Ed. Engl.*, 1979, **18**, 809–826.

9 M. R. Sun, H. L. Li, M. Y. Ba, W. Cheng, H. L. Zhu and Y. T. Duan, *Mini-Rev. Med. Chem.*, 2021, **21**(2), 150–170.

10 Z. Casar, *Synthesis*, 2020, **52**, 1315–1345.

11 M. Yoshida, M. Ezaki, M. Hashimoto, M. Yamashita, N. Shigematsu, M. Okuhara, M. Kohsaka and K. Horikoshi, *J. Antibiot.*, 1990, **43**(7), 748–754.

12 M. Ansseau, *Inpharma Wkly.*, 1989, **698**, 4–5.

13 M. T. Smith, L. E. J. Evans, M. J. Eadie and J. H. Tyrer, *Eur. J. Clin. Pharmacol.*, 1979, **16**, 141–147.

14 D. Chessman, L. Kostenko and T. Lethborg, *et al.*, *Immunity*, 2008, **28**, 822–832.

15 A. J. Rapkin and S. A. Winer, *Expert Opin. Pharmacother.*, 2007, **8**, 989–999.

16 P. Kawalec, J. Kryst, A. Mikrut and A. Pilc, *PLoS One*, 2013, **8**, e76587–e76598.

17 C. D. Bernstein, K. L. Albrecht and D. A. Marcus, *Expert Opin. Pharmacother.*, 2013, **14**, 905–916.

18 O. Burkhardt and T. Welte, *Expert Rev. Anti-infect. Ther.*, 2009, 645–668.

19 S. Amlani, T. Nadarajah and R. A. McIvor, *Expert Opin. Pharmacother.*, 2011, **12**, 2119–2128.

20 M. M. P. Bastos, C. C. Costa, T. C. Bezerra, F. C. Da Silva and N. Boechat, *Eur. J. Med. Chem.*, 2016, **108**, 455–465.

21 A. Corsini and R. Ceska, *Curr. Med. Res. Opin.*, 2011, **27**, 1551–1562.

22 S. Ahmad and R. F. Storey, *Curr. Pharm. Des.*, 2012, **18**, 5240–5260.

23 F. S. Mah and C. M. Sanfilippo, *Ophthalmol. Ther.*, 2016, **5**, 1–20.

24 S. Dhillon, *Drugs*, 2015, **75**, 1783–1796.

25 Z. T. Al-Salama, G. M. Keating and S. J. Keam, *Drugs*, 2017, **77**, 2025–2036.

26 K. P. Garnock-Jones, *Drugs*, 2012, **72**, 2431–2456.

27 C. M. Perry, *Drugs*, 2012, **72**, 619–641.

28 A. Mullard, *Nat. Rev. Drug Discovery*, 2019, **18**, 85–89.

29 N. A. J. Meanwell, *Med. Chem.*, 2018, **61**, 582.

30 Y. Zhou, J. Wang, J. Gu, S. Wang, W. Zhu, J. L. Aceña, V. A. Soloshonok, K. Izawa and H. Liu, *Chem. Rev.*, 2016, **116**, 422–518.

31 A. Gawor, Z. Gajewski, L. Paczek, B. Czarkowska-Paczek, A. Konopka, G. Wryk and E. Bulska, *Int. J. Mol. Sci.*, 2022, **23**, 4202–4213.

32 T. T. Talele, *J. Med. Chem.*, 2016, **59**, 8712–8756.

33 W. Wang, H. Lu, M. Zhang, H. Ma, X. Cheng, Y. Ding and A. Hu, *J. Mater. Chem. B*, 2021, **9**, 4502–4509.

34 H. Lu, Q. Zhou, J. He, Z. Jiang, C. Peng, R. Tong and J. Shi, *Signal Transduct. Target. Ther.*, 2020, **5**, 213–236.

35 D. E. Arthur and J. Uzairu, *J. King Saud Univ., Sci.*, 2019, **31**, 1151–1166.

36 Y. Lee, S. Kim, J. Y. Kim, M. Arooj and S. Kim, *et al.*, *PLoS One*, 2014, **9**(1), e85827.

37 V. Apostolopoulos, J. Bojarska, T. T. Chai, S. Elnagdy, K. Kaczmarek and J. Matsoukas, *et al.*, *Molecules*, 2021, **26**, 430–475.

38 V. Apostolopoulos, J. Bojarska, J. Feehan, J. Matsoukas and W. M. Wolf, *Front. Pharmacol.*, 2022, **13**, 914467–914475.

39 C. H. Stammer, WO1985000809A1, 1985.

40 J. W. Steed and J. L. Atwood, *Supramolecular Chemistry*, John Wiley & Sons, Ltd., UK, 2nd edn, 2009.

41 G. Desiraju, *Angew. Chem., Int. Ed. Engl.*, 1995, **34**, 2311–2327.

42 P. R. Spackman, L. J. Yu, C. J. Morton, M. W. Parker, C. S. Bond and M. A. Spackman, *et al.*, *Angew. Chem.*, 2019, **131**, 16936–16940.

43 J. D. Dunitz, *Pure Appl. Chem.*, 1991, **63**, 177–185.

44 J. Bojarska, M. Breza, M. Remko, M. Czyz, A. Gajos-Michniewicz, M. Zimecki, K. Kaczmarek, I. D. Madura, J. M. Wojciechowski and W. M. Wolf, *Int. J. Mol. Sci.*, 2022, **23**, 7173–7205.

45 V. P. Chavda, J. Ajabiya, D. Teli, J. Bojarska and V. Apostolopoulos, *Molecules*, 2022, **27**, 4315–4325.

46 V. Apostolopoulos, J. Bojarska, T. T. Chai, J. Feehan, K. Kaczmarek, J. M. Matsoukas, O. Paredes Lopez, M. Saviano, M. Skwarczynski and J. Smith-Carpenter, *et al.*, *Molecules*, 2022, **27**, 3635–3639.

47 J. Bojarska, A. Mieczkowski, Z. M. Ziora, M. Skwarczynski, I. Toth, A. O. Shalash, K. Parang, S. A. El-Mowafi, E. H. M. Mohammed and S. Elnagdy, *et al.*, *Biomolecules*, 2021, **11**, 1515–1579.

48 J. Bojarska and W. M. Wolf, *Proceedings*, 2021, **79**(1), 10–18.

49 J. Bojarska, V. Apostolopouos, J. Matsoukas, J. Feehan, H. Ridgway, P. Zielenkiewicz and W. M. Wolf, *Acta Crystallogr., Sect. A: Found. Adv.*, 2021, **77**, c794–c795.

50 J. Bojarska, *Acta Crystallogr., Sect. A: Found. Adv.*, 2021, **77**, c1070.

51 J. Bojarska, *Acta Crystallogr., Sect. A: Found. Adv.*, 2021, **77**, c1210.

52 J. Bojarska, R. New, P. Borowiecki, M. Remko, M. Breza, I. D. Madura, A. Fruzinski, A. Pietrzak and W. M. Wolf, *Front. Chem.*, 2021, **9**, 679776–679800.

53 J. Bojarska, M. Remko, M. Breza, I. D. Madura, A. Fruzinski and W. M. Wolf, *Pharmaceuticals*, 2020, **13**, 338–380.

54 J. Bojarska, *Int. J. Nutr. Sci.*, 2021, **6**(1), 104–108.

55 J. Bojarska, *Int. J. Nutr. Sci.*, 2020, **5**(1), 1039–1044.

56 J. Bojarska, M. Remko, I. D. Madura, K. Kaczmarek, J. Zabrocki and W. M. Wolf, *Acta Crystallogr., Sect. C: Struct. Chem.*, 2020, **76**, 328–345.

57 J. Bojarska, M. Remko, M. Breza, I. D. Madura, K. Kaczmarek and J. Zabrocki, *et al.*, *Molecules*, 2020, **25**, 1135–1162.

58 J. Bojarska, M. Remko, I. D. Madura, J. M. Wojciechowski, A. Olczak and K. Kaczmarek, *et al.*, *J. Mol. Struct.*, 2019, **1190**, 11–22.

59 J. Bojarska, K. Kaczmarek, J. Zabrocki and W. M. Wolf, *Int. J. Nutr. Sci.*, 2019, **4**, 1035–1037.

60 J. Bojarska, A. Fruzinski, L. Sieron and W. Maniukiewicz, *J. Mol. Struct.*, 2019, **1179**, 411–420.

61 J. Bojarska, K. Kaczmarek, J. Zabrocki and W. M. Wolf, *Novel Approaches in Drug Designing and Development*, 2019, **129**, 1–27.

62 J. Bojarska, J. Zabrocki, K. Kaczmarek, M. Remko and W. M. Wolf, *Acta Crystallogr., Sect. A: Found. Adv.*, 2019, **75**, e588.

63 J. Bojarska, K. Kaczmarek, J. Zabrocki and W. M. Wolf, Supramolecular Chemistry of Modified Amino Acids and Short Peptides, in *Advances in Organic Synthesis*, ed. A. Rahman, Bentham Science Publishers Ltd., Sharjah, UAE, 2018, vol. 11, pp. 43–107.

64 J. Bojarska, M. Remko, A. Fruzinski and W. Maniukiewicz, *J. Mol. Struct.*, 2018, **1154**, 290–300.

65 J. Bojarska, A. Fruzinski and W. Maniukiewicz, *J. Mol. Struct.*, 2016, **1116**, 22–29.

66 J. Bojarska and W. Maniukiewicz, *J. Mol. Struct.*, 2015, **1099**, 419–426.

67 J. Bojarska, W. Maniukiewicz, A. Fruzinski, L. Sieron and M. Remko, *Acta Crystallogr., Sect. C: Struct. Chem.*, 2015, **71**, 199–203.

68 J. Bojarska, W. Maniukiewicz, A. Fruzinski, M. Jedrzejczyk, J. Wojciechowski and H. Krawczyk, *J. Mol. Struct.*, 2014, **1076**, 126–135.

69 J. Bojarska, W. Maniukiewicz, M. Glówka, L. Sierón and M. Remko, *J. Chil. Chem. Soc.*, 2013, **58**, 1530–1533.

70 J. Bojarska, W. Maniukiewicz, L. Sieron and M. Remko, *Acta Crystallogr., Sect. C: Cryst. Struct. Commun.*, 2013, **69**, 630–633.

71 J. Bojarska, W. Maniukiewicz and L. Sieron, *Acta Crystallogr., Sect. C: Cryst. Struct. Commun.*, 2013, **69**, 781–786.

72 J. Bojarska, W. Maniukiewicz, L. Sieron, A. Fruzinski, P. Kopczacki and K. Walczynski, *et al.*, *Acta Crystallogr., Sect. C: Cryst. Struct. Commun.*, 2012, **68**, o341–o343.

73 J. Bojarska, W. Maniukiewicz, L. Sieron, P. Kopczacki, K. Walczynski and M. Remko, *Acta Crystallogr., Sect. C: Cryst. Struct. Commun.*, 2012, **68**, o443–o446.

74 A. Olczak, M. Glówka, M. Szczesio, J. Bojarska, W. L. Duax and B. M. Burkhart, *et al.*, *Acta Crystallogr., Sect. D: Biol. Crystallogr.*, 2007, **63**, 319–327.

75 A. Olczak, M. L. Glówka, M. Szczesio, J. Bojarska, Z. Wawrzak and W. L. Duax, *Acta Crystallogr., Sect. D: Biol. Crystallogr.*, 2010, **66**, 874–880.

76 M. Glówka, A. Olczak, J. Bojarska, M. Szczesio, W. L. Duax and B. M. Burkhart, *Acta Crystallogr., Sect. D: Biol. Crystallogr.*, 2005, **61**, 433–441.

77 M. Glówka, A. Olczak, J. Bojarska, M. Szczesio, W. L. Duax and B. Burkhart, *et al.*, *Acta Crystallogr., Sect. A: Found. Crystallogr.*, 2004, **60**, 165.

78 M. Glówka, A. Olczak, J. Bojarska and M. Szczesio, *J. Polish Chem. Soc.*, 2007, **61**, 161–187.

79 J. Bojarska, L. Sieron and W. Maniukiewicz, *Struct. Chem.*, 2018, **29**, 1525–1531.

80 M. Remko, J. Bojarska, A. Remková and W. Maniukiewicz, *Comput. Theor. Chem.*, 2015, **1062**, 50–55.

81 M. Remko, J. Bojarska, P. JEzko, W. Maniukiewicz and A. Olczak, *J. Mol. Struct.*, 2013, **1036**, 292–297.

82 M. Remko, J. Bojarska, P. Jezko, L. Sieron, A. Olczak and W. Maniukiewicz, *J. Mol. Struct.*, 2011, **997**, 103–109.

83 C. Hamon and B. J. Rawlings, *Synth. Commun.*, 1996, **26**(6), 1109–1115.

84 O. V. Dolomanov, L. J. Bourhis, R. J. Gildea, J. A. K. Howard and H. Puschmann, *J. Appl. Crystallogr.*, 2009, **42**, 339–341.

85 G. M. Sheldrick, *Acta Crystallogr., Sect. A: Found. Adv.*, 2015, **71**, 3–8.

86 *CrysAlisPRO*, Oxford Diffraction/Agilent Technologies UK Ltd, Yarnton, England.

87 G. M. Sheldrick, *Acta Crystallogr., Sect. C: Struct. Chem.*, 2015, **71**, 3–8.

88 A. L. Spek, *Acta Crystallogr., Sect. D: Biol. Crystallogr.*, 2009, **65**, 148–155.

89 C. F. Macrae, I. J. Bruno, J. A. Chisholm, P. R. Edgington, P. McCabe and E. Pidcock, *et al.*, *J. Appl. Crystallogr.*, 2008, **41**, 466–470.

90 C. F. MacRae, I. Sovago, S. J. Cottrell, P. T. A. Galek, P. McCabe, E. Pidcock, M. Platings, G. P. Shields, J. S. Stevens, M. Towler and P. A. Wood, *J. Appl. Crystallogr.*, 2020, **53**, 226–235.

91 C. R. Groom, I. J. Bruno, M. P. Lightfoot and S. C. Ward, *Acta Crystallogr., Sect. B: Struct. Sci., Cryst. Eng. Mater.*, 2016, **72**, 171–179.

92 M. J. Frisch, G. W. Trucks, H. B. Schlegel, G. E. Scuseria, M. A. Robb, J. R. Cheeseman, G. Scalmani, V. Barone, B. Mennucci, G. A. Petersson, H. Nakatsuji, M. Caricato, X. Li, H. P. Hratchian, A. F. Izmaylov, J. Bloino, G. Zheng, J. L. Sonnenberg, M. Hada, M. Ehara, K. Toyota, R. Fukuda, J. Hasegawa, M. Ishida, T. Nakajima, Y. Honda, O. Kitao, H. Nakai, T. Vreven, J. A. Montgomery Jr., J. E. Peralta, F. Ogliaro, M. Bearpark, J. J. Heyd, E. Brothers, K. N. Kudin, V. N. Staroverov, R. Kobayashi, J. Normand, K. Raghavachari, A. Rendell, J. C. Burant, S. S. Iyengar, J. Tomasi, M. Cossi, N. Rega, J. M. Millam, M. Klene, J. E. Knox, J. B. Cross, V. Bakken, C. Adamo, J. Jaramillo, R. Gomperts, R. E. Stratmann, O. Yazyev, A. J. Austin, R. Cammi, C. Pomelli, J. W. Ochterski, R. L. Martin, K. Morokuma, V. G. Zakrzewski, G. A. Voth, P. Salvador, J. J. Dannenberg, S. Dapprich, A. D. Daniels, Ö. Farkas, J. B. Foresman, J. V. Ortiz, J. Cioslowski and D. J. Fox, *Gaussian 09, Version 9.0*, Gaussian Inc., Wallingford, CT, 2011.

93 R. G. Parr and W. Wang, *Density-Functional Theory of Atoms and Molecules*, Oxford University Press, New York, 1994.

94 R. Neumann, R. H. Nobes and N. C. Handy, *Mol. Phys.*, 1996, **87**, 1–36.

95 F. M. Bickelhaupt and E. J. Baerends, in *Rev. Comput. Chem.*, ed. K. B. Lipkowitz and D. B. Boyd, Wiley-VCH, New York, 2000, vol. 15, pp. 1–86.

96 Y. Zhao and D. G. Truhlar, *Theor. Chem. Acc.*, 2008, **120**, 215–241.

97 W. J. Hehre, L. Radom, P. V. R. Schleyer and J. A. Pople, *Ab Initio Molecular Orbital Theory*, Wiley, New York, 1986.

98 A. E. Reed, L. A. Curtiss and F. Weinhold, *Chem. Rev.*, 1988, **88**, 899–926.

99 P. P. Graczyk and M. Mikołajczyk, *Topics in Stereochemistry*, ed. E. L. Eliel and S. H. Wilen, Wiley, New York, 1994, vol. 21, pp. 159–349.

100 H. Krawczyk, K. Wasek, J. Kedzia, J. Wojciechowski and W. M. Wolf, *Acta Crystallogr., Sect. C: Cryst. Struct. Commun.*, 2008, **64**, o24–o26.

101 F. Biegler-Konig, J. Schonbohm and D. Bayles, *J. Comput. Chem.*, 2001, **22**, 545–559.

102 R. F. W. Bader, *Atoms in molecules—a quantum theory*, Oxford University Press, Oxford, 1990.

103 M. A. Spackman and J. J. McKinnon, *CrystEngComm*, 2002, **4**, 378–392.

104 M. A. Spackman, J. J. McKinnon and D. Jayatilaka, *CrystEngComm*, 2008, **10**, 377–388.

105 S. P. Thomas, P. R. Spackman, D. Jayatilaka and M. A. Spackman, *J. Chem. Theory Comput.*, 2018, **14**, 1614–1623.

106 C. F. MacKenzie, P. R. Spackman, D. Jayatilaka and M. A. Spackman, *IUCrJ*, 2017, **4**(5), 575–587.

107 P. R. Spackman, M. J. Turner, J. J. McKinnon, S. K. Wolff, D. J. Grimwood, D. Jayatilaka and M. A. Spackman, *J. Appl. Crystallogr.*, 2021, **54**, 1006–1011.

108 D. Jayatilaka and D. J. Grimwood, *Lect. Notes Comput. Sci. (including Subser. Lect. Notes Artif. Intell. Lect. NotesBioinformatics)*, 2003, vol. 2660, pp. 142–151.

109 A. Daina and V. A. Zoete, *ChemMedChem*, 2016, **11**, 1117–1121.

110 A. Daina, O. Michielin and V. Zoete, *Sci. Rep.*, 2017, **7**, 42717–42730.

111 D. E. V. Pires, T. L. Blundell and D. B. Ascher, *J. Med. Chem.*, 2015, **58**, 4066–4072.

112 R. C. Braga, V. M. Alves, M. F. B. Silva, E. Muratov, D. Fourches, L. M. Liao, A. Tropsha and C. H. Andrade, *Mol. Inf.*, 2015, **34**, 698–701.

113 A. A. Lagunin, V. I. Dubovskaja, A. V. Rudik and P. V. Pogodin, *et al.*, *PLoS One*, 2018, **13**, e0191838–e0191852.

114 A. Avdeef, *Anal. Chim. Acta*, 1983, **148**, 237–244.

115 A. Avdeef and J. Comer, *J. Pharm. Sci.*, 1993, **82**, 183–190.

116 K. Y. Tam and K. Takacs-Novak, *Anal. Chim. Acta*, 2001, **434**, 157–167.

117 A. Avdeef, J. Comer and S. J. Thomson, *Anal. Chem.*, 1993, **65**, 42–49.

118 H. Putz and K. Brandenburg, *Diamond, Crystal and Molecular Structure Visualization, Crystal Impact GbR*, Kreuzherrenstr. 102, D-53227 Bonn, Germany.

119 A. Osipova, D. S. Yufit and A. de Meijere, *Synthesis*, 2007, **2007**, 131–139.

120 W. Huang and F. Meng, *Angew. Chem.*, 2021, **60**, 2694–2698.

121 G. Kang, J. Kim, E. Kwon and T. H. Kim, *Acta Crystallogr., Sect. E: Crystallogr. Commun.*, 2015, **71**, o631–o632.

122 L. Qin, L. Ren, S. Wan, G. Liu, X. Luo, Z. Liu, F. Li, Y. Yu, J. Liu and Y. Wei, *J. Med. Chem.*, 2017, **60**, 3606–3617.

123 F. Brackman and A. de Meijere, *Synthesis*, 2005, **12**, 2008–2014.

124 Z. Q. Sun, Z. Y. Ding and Z. Y. Shao, *Acta Crystallogr., Sect. E: Struct. Rep. Online*, 2012, **68**, o3029–o3030.

125 B. Liu and L. Tian, *Acta Crystallogr., Sect. E: Struct. Rep. Online*, 2006, **62**, o4280–o4281.

126 N. Rowles, H. G. Heller, D. S. Hughes and M. B. Hursthouse, *CSD Communication (Private Communication)*, 2012.

127 S. M. Wales, E. G. Merisor, H. V. Adcock, C. A. Pearce, I. R. Strutt, W. Lewis, D. Hamza and C. J. Moody, *Chem. – Eur. J.*, 2018, **24**, 8233–8239.

128 L. Tian and B. Liu, *Acta Crystallogr., Sect. E: Struct. Rep. Online*, 2006, **62**, o4183–o4184.

129 H. Y. Bai, X. Fu, J. L. Pan, H. Q. Ma, Z. M. Chen, T. M. Ding and S. Y. Zhang, *Adv. Synth. Catal.*, 2018, **360**, 4205–4214.

130 R. Hartung, G. Golz, S. Schlaf, G. Silvenoinen, K. Polborn, P. Mayer and H. R. Pfaendler, *Synthesis*, 2009, **2009**, 495–501.

131 P. Sivaprakasam, X. Han, R. L. Civiello, S. Jacutin-Porte, K. Kish and M. Pokross, *et al.*, *Bioorg. Med. Chem. Lett.*, 2015, **25**, 1856–1863.

132 P. G. Jones, A. J. Kirby and R. J. Lewis, *Acta Crystallogr., Sect. C: Cryst. Struct. Commun.*, 1990, **46**, 78–81.

133 D. V. B. Walji, J. M. D. Storey and W. T. A. Harrison, *Acta Crystallogr., Sect. E: Struct. Rep. Online*, 2007, **63**, o1761–o1762.

134 G. Bradley, T. J. Ward, J. C. White, J. Coleman, A. Taylor and K. F. Rhodes, *J. Med. Chem.*, 1992, **35**, 1515–1520.

135 M. H. Qi, Q. D. Zhang, Y. Liu, F. Z. Ren and G. B. Ren, *J. Mol. Struct.*, 2019, **1178**, 242–250.

136 H. G. Heller, D. S. Hughes, M. B. Hursthouse and N. G. Rowles, *Chem. Commun.*, 2000, 1397–1398.

137 J. Chen, B. Q. Huang, Z. Q. Wang, X. J. Zhang and M. Yan, *Org. Lett.*, 2019, **21**, 9742–9746.

138 M. Viertelhaus, H. C. Holst, J. Volz and R. P. Hummel, *J. Mol. Struct.*, 2013, **1031**, 254–262.

139 C. Sen, T. Sahoo, H. Singh, E. Suresh and S. C. Ghosh, *J. Org. Chem.*, 2019, **84**, 9869–9896.

140 M. W. D. Perry, A. Eriksson and M. R. Landergren, *Tetrahedron: Asymmetry*, 2017, **28**, 1135–1138.

141 L. Tian, B. Liu and J. Wang, *Acta Crystallogr., Sect. E: Struct. Rep. Online*, 2007, **63**, o273–o274.

142 Z. Liu, F. Huang, P. Wu, Q. Wang and Z. Yu, *J. Org. Chem.*, 2018, **83**, 5731–5750.

143 A. Guelzim, E. Belloli, S. Yous and C. Vaccher, *Acta Crystallogr., Sect. C: Cryst. Struct. Commun.*, 2001, **57**, 100–101.

144 M. C. Hiller, J. P. Davidson and S. F. Martin, *J. Org. Chem.*, 2011, **66**, 1657–1671.

145 R. W. Driver, T. D. W. Claridge, S. Scheiner and M. D. Smith, *Chem. – Eur. J.*, 2016, **22**, 16513–16521.

146 R. Perez-Ruiz, J. A. Saez, L. R. Domingo, M. C. Jimenez and M. A. Miranda, *Org. Biomol. Chem.*, 2012, **10**, 7928–7932.

147 S. J. Lee, J. Y. Bae and C. W. Cho, *Eur. J. Org. Chem.*, 2015, **2015**, 6495–6502.

148 J. F. Malone, C. M. Murray, M. H. Charlton, R. Docherty and A. J. Lavery, *J. Chem. Soc., Faraday Trans.*, 1997, **93**, 3429–3436.

149 P. Ganguly and G. R. Desiraju, *CrystEngComm*, 2010, **12**, 817–833.

150 A. I. Kitaigorodskii, *Organic chemical crystallography*, Consultants Bureau, New York, 1961.

151 C. P. Brock, *Acta Crystallogr., Sect. B: Struct. Sci., Cryst. Eng. Mater.*, 2016, **72**, 807–821.

152 C. Jelsch, K. Ejsmont and L. Huder, *IUCrJ*, 2014, **1**, 119–128.

153 J. P. Foster and F. Weinhold, *J. Am. Chem. Soc.*, 1980, **102**, 7211–7218.

154 D. T. Manallack, *Perspect. Med. Chem.*, 2017, **1**, 25–38.

155 A. Daina, O. Michielin and V. Zoete, *Nucleic Acids Res.*, 2019, **47**, w357–w364.

156 G. K. Gupta and V. Kumar, *Chemical Drug Design*, Walter de Gruyter GmbH, Berlin, Germany, 2016.

157 S. Sumanasuriya and J. De Bono, *Cold Spring Harbor Perspect. Med.*, 2018, **8**, a030635.

158 H. Suzuki, T. Ueda, T. Ichikawa and H. Ito, *Endocr.-Relat. Cancer*, 2003, **10**, 209–216.